Potassium Buffering in the Neurovascular Unit: Models and Sensitivity Analysis

Alexandra Witthoft,[†] Jessica A. Filosa,[‡] and George Em Karniadakis[§*]
[†]School of Engineering, Brown University, Providence, Rhode Island; [‡]Department of Physiology, Georgia Regents University, Augusta, Georgia; and [§]Division of Applied Mathematics, Brown University, Providence, Rhode Island

ABSTRACT Astrocytes are critical regulators of neural and neurovascular network communication. Potassium transport is a central mechanism behind their many functions. Astrocytes encircle synapses with their distal processes, which express two potassium pumps (Na-K and NKCC) and an inward rectifying potassium channel (Kir), whereas the vessel-adjacent endfeet express Kir and BK potassium channels. We provide a detailed model of potassium flow throughout the neurovascular unit (synaptic region, astrocytes, and arteriole) for the cortex of the young brain. Our model reproduces several phenomena observed experimentally: functional hyperemia, in which neural activity triggers astrocytic potassium release at the perivascular endfoot, inducing arteriole dilation; K^+ undershoot in the synaptic space after periods of neural activity; neurally induced astrocyte hyperpolarization during Kir blockade. Our results suggest that the dynamics of the vascular response during functional hyperemia are governed by astrocytic Kir for the fast onset and astrocytic BK for maintaining dilation. The model supports the hypothesis that K^+ undershoot is caused by excessive astrocytic uptake through Na-K and NKCC pumps, whereas the effect is balanced by Kir. We address parametric uncertainty using high-dimensional stochastic sensitivity analysis and identify possible model limitations.

INTRODUCTION

The conventional view of the brain has long been a large network of neurons. Other cerebral cell types and vasculature were originally considered to have supporting roles. It is now accepted that astrocytes (a specific type of glial cell) and cerebral vasculature may play a critical role in neural behavior, giving rise to the idea of a neurovascular unit (NVU). Astrocytes are believed to mediate neurovascular coupling, also called functional hyperemia, the phenomenon in which synaptic activity induces dilation in nearby microvasculature, allowing increased blood flow.

A central function of cerebral astrocytes is spatial potassium (K^+) buffering, that is, transporting K^+ from extracellular regions of high concentration to regions of low concentration via active uptake and release. Uptake usually occurs at the astrocyte-neural interface, where active neurons release K^+, which at high extracellular levels can be excitatory to neurons; release typically occurs at the perivascular space, the extracellular region between the astrocyte endfoot and the abluminal surface of an arteriole, which dilates in response to K^+. Thus, the buffering is a regulatory mechanism that both protects neurons from excessive excitation and dilates arterioles to increase blood supply to areas of increased neural activity. There may also be a functional role, as changes to extracellular K^+ can increase or decrease synaptic activity. To study the neurovascular unit as an interconnected, interactional system, a quantitative mechanistic understanding of K^+ spatial buffering is critical.

We recently developed a model of the neurovascular unit (1) that described a two-way signaling pathway: in one direction, astrocytes are stimulated by synaptic activity, with subsequent arteriole dilation, and in the reverse direction, vessel motion triggers astrocyte calcium response through activation of mechanosensors on the astrocyte endfoot. Although that astrocyte model included K^+ movement from the synaptic to the perivascular space, the movement was a unidirectional flux and did not describe intracellular K^+ dynamics.

Astrocytes express potassium inward rectifier (Kir) channels on their perisynaptic processes and perivascular endfeet (2–8), and these channels have been reported to play a major role in the potassium uptake and release involved in spatial buffering. Calcium-sensitive BK channels in the perivascular endfeet are also a critical means of potassium release (9–11). There are also active K^+ uptake mechanisms in the perisynaptic processes, including a sodium-potassium (Na-K) pump and a sodium-potassium-chloride cotransport (NKCC) (12–15).

There have been some computational studies of potassium buffering in the brain, but many include only simplistic, lumped cellular models and exclude most other chemical and electrical mechanisms (16–18). Models of the astrocyte-neural interface, the tripartite synapse (19), omit the vascular component and focus primarily on detailed neural mechanisms (12,15,20), whereas we are interested in an explicit description of the astrocyte.

We present a model of the neurovascular unit in the cortex with a detailed mechanistic description of astrocytic potassium buffering. This model describes the potassium dynamics in the astrocyte intracellular space and in the

Submitted May 31, 2013, and accepted for publication September 10, 2013.
*Correspondence: George_Karniadakis@brown.edu
Editor: Randall Rasmusson.

0006-3495/13/11/2046/9 $2.00
http://dx.doi.org/10.1016/j.bpj.2013.09.012

extracellular spaces at the synaptic and perivascular interfaces. Astrocyte potassium uptake at the synaptic space is carried by potassium inward rectifier (Kir) channels, potassium-sodium (Na-K) exchange, and a potassium-sodium-chloride cotransporter (NKCC) on the astrocyte perisynaptic process. From here on, Kir_{AS} refers to the Kir channel on the astrocyte at the synapse-adjacent process. The perivascular endfoot expresses Kir, here referred to as Kir_{AV}, for astrocytic at the vessel-adjacent endfoot, and calcium-sensitive BK channels. Although astrocytes express other ion channels, these are not included explicitly, but are accounted for collectively by a nonspecific leak channel. This model is specific to cortical astrocytes in the developing brain, as we discuss further below.

This article is organized as follows. In the Mathematical Model section, we provide new equations developed for the model presented here. In the Results section, we compare the results of our simulation to results of several different experimental studies. In the Sensitivity Analysis section, we examine the results of global parameter sensitivity analysis of the astrocyte model. In the Discussion section, we comment on the implications of the simulations and sensitivity analysis and describe the limitations of the model and plans for future work. In the Supporting Material, we present additional sensitivity analysis results, and we describe in detail the complete set of model equations and parameter values.

MATHEMATICAL MODEL

A conceptual diagram of the model is shown in Fig. 1. The model equations concern the small spatial region of the developing brain cortex occupied by a single astrocyte and the synapses and arteriole segment with which it is in contact. Astrocyte-to-astrocyte signaling is left out, and the synaptic space represents the net neural synaptic activity across the entire astrocyte domain, which is assumed to be spatially uniform within the region.

During high synaptic activity, neurons release K^+ and glutamate at the synapses (Ω_S). K^+ flows into the adjacent astrocytic process through Kir_{AS} channels, Na-K, and NKCC on the perisynaptic process. The Na-K pump exchanges three sodium (Na^+) ions for two K^+ ions. The NKCC is an electrically neutral import of one Na^+ ion, one K^+ ion, and two Cl^- ions; however, the Na^+ intake affects the Na-K pump activity, which is hyperpolarizing. The Kir_{AS} current is larger in magnitude than the outward Na^+ current from the Na-K pump, resulting in an overall depolarization of the astrocyte membrane. The NKCC and Na-K pumps have slow dynamics, making them potentially less efficient for K^+ buffering. Still, they are likely critical to the astrocyte's role in regulating K^+ in the synaptic space (see Results, below).

Cortical astrocytes in young brains express on their perisynaptic processes (Ω_{Astr}) glutamate receptors (mGluR5) that initiate intracellular IP_3 production in response to synaptic glutamate release. IP_3 binds to receptors (IP_3R) on the endoplasmic reticulum (ER), releasing calcium (Ca^{2+}) from internal stores. This is most likely specific to astrocytes in the young brain, as Sun et al. (21) recently found that mGluR5 is expressed in cortical and hippocampal astrocytes from young (<2 weeks old) mice brains, but not in adult mouse or human brains, and, further, that glutamate-dependent astrocytic Ca^{2+} rises may be unlikely in the adult brain.

The mGluR5-dependent rise in intracellular Ca^{2+} enables production of epoxyeicosatrienoic acids (EETs). EET and Ca^{2+} activate BK channels in the astrocyte endfoot, releasing K^+ into the perivascular space (Ω_P). It is unclear whether EET acts directly on the BK channels; it may act indirectly by activating TRPV4 channels (22,23). This would result in a Ca^{2+} influx and membrane depolarization, both of which activate BK channels. For the moment, we

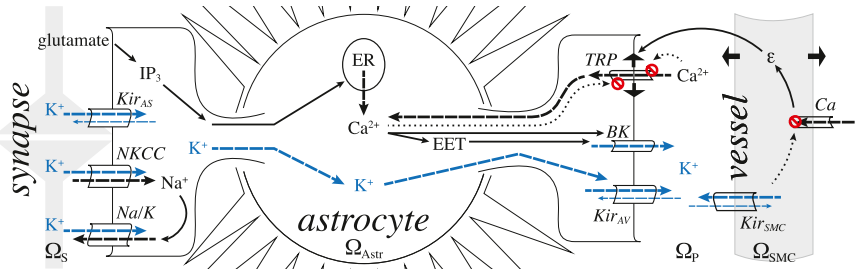

FIGURE 1 Model overview. Ω_S represents the synaptic space, where active synapses release glutamate and K^+, and Ω_{Astr} is the astrocyte intracellular space, where K^+ enters the astrocyte through the Na-K pump, NKCC, and Kir_{AS} channels. Na^+ enters via NKCC and exits via the Na-K pump. Glutamate binds to metabotropic receptors on the astrocyte endfoot, effecting IP_3 production inside the astrocyte wall, which leads to release of Ca^{2+} from internal stores, causing EET production. Ca^{2+} and EET open BK channels at the perivascular endfoot, releasing K^+ into the perivascular space (Ω_P). Meanwhile, buildup of intracellular K^+ in the astrocyte results in K^+ efflux through the perivascular endfoot Kir_{AV} channel. Ω_{SMC} is the arteriole smooth muscle cell intracellular space, where Kir_{SMC} channels are activated by the increase in extracellular K^+. The resulting drop in membrane potential closes Ca^{2+} channels, which reduces Ca^{2+} influx, leading to SMC relaxation and arteriole dilation (strain, ϵ). The arteriole dilation (ϵ) stretches the membrane of the enclosing astrocyte perivascular endfoot, which activates Ca^{2+} influx through TRPV4 channels. The prohibition sign on the channel is meant to indicate the inhibition mechanism of the channel, as the TRPV4 channel is inhibited by intracellular and extracellular Ca^{2+}. Note that the diagram here is not to scale. The perivascular endfoot is actually wrapped around the arteriole, but here we show them separated to make clear the ion flow at the endfoot-vessel interface. Dashed arrows indicate ion movement; solid arrows indicate causal relationships, and dotted arrows indicate inhibition. Thin dashed arrows in astrocyte Kir channels indicate the ion flux direction at baseline or, in the vessel Kir, the change in flux direction when extracellular K^+ reaches over 15 mM. The potassium signaling pathway is highlighted by blue arrows. To see this figure in color, go online.

follow the model of Farr and David (24) which is an empirical description of the relationship between EET and BK activity, but a more mechanistic description can be added later as more data become available. K^+ is also released through the endfeet Kir_{AV} channels.

The K^+ buildup in the perivascular space activates arteriolar smooth muscle cell (SMC) Kir channels, referred to from here on as Kir_{SMC} (Ω_{SMC}). The resting SMC membrane potential is higher than the Kir_{SMC} reversal potential, so the K^+ flows outward. The resulting SMC membrane voltage drop closes inward Ca^{2+} channels, and the intracellular Ca^{2+} concentration in the SMC drops. Because Ca^{2+} is required for myosin-actin cross-bridge attachment, the cross-bridges then detach, allowing the SMC to relax and the arteriole to expand.

As the vessel dilates, it stretches the perivascular astrocyte endfoot encircling it (Ω_{Astr}), opening stretch-gated Ca^{2+}-permeable TRPV4 channels in the endfoot. TRPV4 channels are also sensitive to intra- and extracellular Ca^{2+} concentration (25–27). There is experimental evidence that TRPV4 channels are activated by a diverse range of chemical and physical factors, including heat (23,25,26,28), EET, and IP_3 (22,27), and they are modulated by phosphorylation (23,27); for simplicity, we leave these mechanisms out for the moment. A more detailed discussion on the TRPV4 model can be found in Witthoft and Karniadakis (1). The astrocyte then experiences a depolarizing Ca^{2+} influx through active TRPV4, thus maintaining BK activation, which prolongs the K^+ signal (Ω_P) to the arteriole (Ω_{SMC}).

Below, we summarize the new, to our knowledge, ordinary differential equations we have developed and added to this model. The complete, detailed system of model equations is given in the Supporting Material.

We describe the neurovascular K^+ movement between three regions in the NVU: the synaptic space, astrocytic intracellular space, and perivascular space. Potassium concentrations in these regions obey

$$\frac{d[K^+]_S}{dt} = J_{K_s} - (J_{NaK,K} + J_{NKCC} + J_{Kir,AS}) \times \frac{1}{VR_{sa}} - Rdc_{K^+,S}\left([K^+]_S - [K^+]_{S,0}\right), \quad (1)$$

in the synaptic space,

$$\frac{d[K^+]_A}{dt} = J_{NaK,K} + J_{NKCC} + J_{Kir,AS} + J_{BK} + J_{Kir,AV} - Rdc_{K^+,A}\left([K^+]_A - [K^+]_{A,0}\right), \quad (2)$$

in the astrocyte intracellular space, and

$$\frac{d[K^+]_{PV}}{dt} = -\frac{J_{BK}+J_{Kir,AV}}{VR_{pa}} - \frac{J_{Kir,SMC}}{VR_{ps}} - R_{dc}\left([K^+]_{PV} - [K^+]_{P,0}\right), \quad (3)$$

in the perivascular space. The individual flux terms and parameters are all discussed in detail in Eqs. S4–S41 in the Supporting Material, but we discuss below the astrocytic flux terms that we have introduced to this model.

The flux from the NKCC is adapted from Østby et al. (15):

$$J_{NKCC} = J_{NKCC,max} \log\left[\frac{[K^+]_S}{[K^+]_A}\frac{[Na^+]_S}{[Na^+]_A}\left(\frac{[Cl^-]_S}{[Cl^-]_A}\right)^2\right], \quad (4)$$

where the subscripts S and A refer to the synaptic and astrocytic spaces, respectively (for more details on the NKCC flux equation, see Eqs. S7 and S8).

The Kir fluxes at the perisynaptic process and perivascular endfoot, $J_{Kir,AS}$ and $J_{Kir,AV}$, respectively, are

$$I_{Kir,AV/S} = g_{Kir,AV/S}\left(V_A - V_{Kir,AV/S}\right), \quad (5)$$

where AV and AS stand for the astrocyte vessel-adjacent endfoot and synapse-adjacent process, respectively. The ionic flux, J, is computed from the electrical current, I, as $J_{Kir} = I_{Kir}/(C_{ast}\gamma)$, where C_{ast} is the astrocyte cell capacitance, and γ is a scaling factor for relating the net movement of ion fluxes to the membrane potential (29). The conductance and reversal potential, $g_{Kir,AV/S}$ and $V_{Kir,AV/S}$ are

$$g_{Kir,AV/S} = g_{Kir,V/S}\sqrt{[K^+]_{PV/S}}, \text{ and } V_{Kir,AV/S} = E_{Kir,endfoot/proc} \log\frac{[K^+]_{PV/S}}{[K^+]_A}, \quad (6)$$

where $[K^+]_{PV/S}$ is the potassium concentration (mM) in the perivascular/synaptic space, and $g_{Kir,V/S}$ is a proportionality constant. $E_{Kir,endfoot}$ and $E_{Kir,proc}$ are the Nernst constants for the astrocyte Kir_{AS} and Kir_{AV} channels, respectively (~25 mV (16)).

RESULTS

Effect of astrocyte K^+ buffering on neurovascular coupling

We simulate neural activation of the astrocyte by imposing a smooth pulse of extracellular glutamate and K^+ in the synaptic space to approximate neural stimulation. In this section, we consider two extracellular regions: 1), the vessel/astrocyte interface (perivascular space), where K^+ buffering helps determine the dynamics of functional hyperemia, and 2), the astrocyte/neural interface, where the astrocyte modulates the extracellular environment in the synaptic space.

Astrocyte/vessel interaction

In this model, the introduction of the astrocytic Kir channels allows the astrocyte to respond to changes in extracellular

and intracellular potassium concentration. To understand how Kir_{AS} and Kir_{AV} channels impact the neurovascular interaction, we compare the results of this model with a lumped version that does not include astrocytic Kir. In the lumped version, we remove the astrocyte Kir current ($J_{Kir,AS} = J_{Kir,AV} = 0$), and instead describe the total membrane current at the synapse-adjacent side of the astrocyte, I_{AS}, as a lumped model for the combination of currents from the Na-K pump and Kir_{AS} and Kir_{AV} channels: $I_{AS} = I_{Kir,AS} + I_{NaK,K} + I_{NaK,Na} \approx I_{NaK,K}$ (see Eqs. S4–S6), similar to the models developed by Witthoft and Karniadakis (1) and Farr and David (24). We adjust the lumped model's leak current (see Eq. S20) so that the baseline and maximum astrocyte membrane potential match those of the detailed buffering model that includes Kir_{AS} and Kir_{AV}.

Fig. 2 shows the effect of astrocyte Kir channels on the NVU under normal conditions (*black curves*), and with the astrocyte Kir_{AS} and Kir_{AV} removed, that is, $I_{Kir,S}$ and $I_{Kir,V}$ are both set to 0, and using the lumped model equation above (*gray curves*). The system experiences a brief period of neural activity (Fig. 2 *a*, *black and gray curves* show synaptic K^+; thin, *red curve* shows glutamate transient), triggering astrocyte membrane depolarization and intracellular K^+ increase (Fig. 2 *b*, *dashed* and *solid curves*, respectively). The glutamate initiates IP_3 production in the astrocyte (Fig. 2 *c*), leading to release of Ca^{2+} from internal stores (Fig. 2 *d*) and causing EET production (Fig. 2 *e*). The astrocytic Ca^{2+} and EET activate BK channels in the astrocyte endfeet (Fig. 2 *f*, *dashed curves*) where K^+ is released into the perivascular space (Fig. 2 *g*). Meanwhile, the membrane depolarization and the increase in intracellular astrocyte K^+ results in an outward K^+ flux through the endfoot Kir_{AV} channels (Fig. 2 *f*, *dash-dotted curve*). In the absence of astrocyte Kir_{AS} and Kir_{AV}, astrocyte K^+ release into the perivascular space is delayed, causing a delay in the vascular response (Fig. 2 *h*). According to the simulation results, this is because the Kir_{AV} is responsible for the immediate release of K^+, whereas the BK current rises later (Fig. 2 *f*). This may explain why previous generations of this astrocyte model, without a description of K^+ buffering or astrocyte Kir channels (24), produced a nonphysiological delay of ~25 s in the neurovascular response.

In the black curves, there is a short period of arteriole constriction during the neural stimulation period (Fig. 2 *h*): at ~25 s, where the radius stops increasing and the vessel begins to constrict. This is a phenomenon observed by Girouard et al. (11) in which moderate increases in extracellular K^+ cause vasodilation, but increases beyond ~15 mM will cause the vessel to constrict. The results are also consistent with the simulations of Farr and David (24), who postulated that the change from dilation to constriction during sustained activity was caused by the arteriole Kir_{SMC} channels, which have a reversal potential that experiences a depolarizing shift with increasing extracellular potassium: when the extracellular K^+ rises above 15 mM, the Kir_{SMC} reversal potential shifts from below to above the SMC membrane potential, reversing the direction of the current, which causes a depolarization that reopens Ca^{2+} channels, in turn causing constriction. This model is discussed in more detail in Farr and David (24).

Astrocyte/neuron interface: extracellular K^+ undershoot

Fig. 3 shows the extracellular K^+ concentration in the synaptic space over a cycle of stimulation and recovery for several different lengths of stimulus time (simulations in Fig. 3 *a* are compared with experimental results from Chever et al. (5), interpolated in Fig. 3 *b*). In the poststimulus recovery period, the extracellular K^+ initially displays a fast drop to below baseline level before returning gradually to the resting-state equilibrium concentration. This undershoot is more pronounced as the length of the stimulation period increases: note that the 60 s stimulus in the top plot results in the greatest

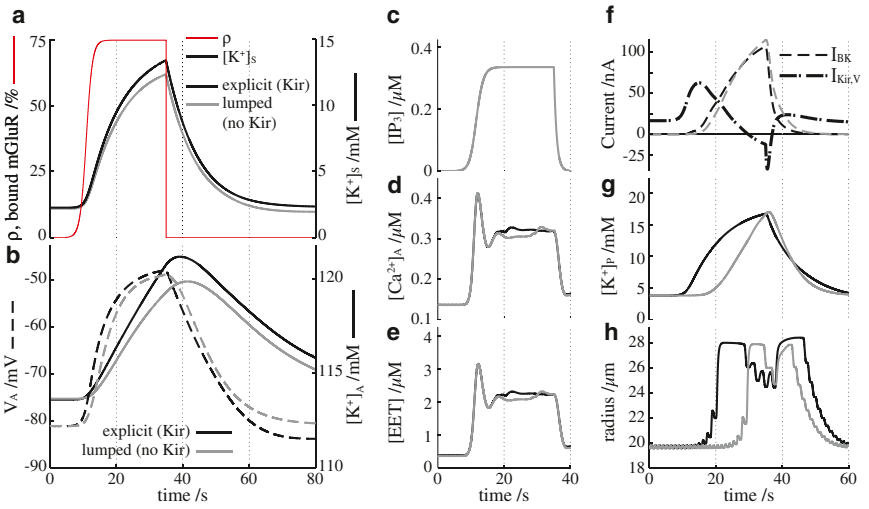

FIGURE 2 Astrocyte Kir effect on neurovascular coupling. Black curves represent the astrocyte model equations described in this article; gray curves represent the astrocyte model equations without Kir_{AS} or Kir_{AV} channels. (*a*) Extracellular K^+ in the synaptic space. The thin red curve is the glutamate transient, represented by the ratio of bound to unbound glutamate receptors, ρ (see Eq. S2). (*b*) Solid lines indicate the intracellular astrocytic K^+ concentration and dashed lines the astrocyte membrane potential. (*c*) Astrocyte intracellular IP_3 concentration. (*d*) Astrocyte intracellular Ca^{2+} concentration. (*e*) Astrocyte intracellular EET concentration. (*f*) Astrocyte perivascular endfoot BK (*dashed lines*) and Kir_{AV} (*dash-dotted lines*) currents. (*g*) Extracellular K^+ concentration in the perivascular space. (*h*) Arteriole radius. To see this figure in color, go online.

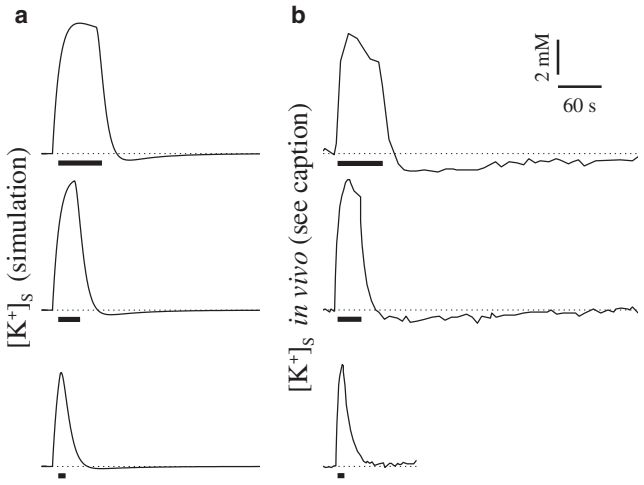

FIGURE 3 K^+ undershoot in the extracellular synaptic space after stimulus is more pronounced with increasing length of the activation period. The stimulus period is indicated by thick black bars. (*a*) Simulation results. (*b*) Experimental results interpolated from Fig. 3 in Chever et al. (5).

undershoot and the longest period of recovery to baseline. With decreasing length of the activation period (*top to bottom*), the undershoot magnitude and recovery time also decrease, a trend that has been reported from in vivo studies in the mouse hippocampus (5). The same experiments also validate the time-dependent characteristics of the undershoot: a fast drop with a slow return to baseline.

Our model suggests that the undershoot is a result of the activities of the Na-K pump and NKCC. The astrocyte Na-K pump flux is an inward movement of K^+ from the synaptic space and an outward flow of Na^+ and is activated by high extracellular K^+ and high intracellular Na^+. Meanwhile, the NKCC flux is an inward K^+ and Na^+ flux that increases with decreasing concentrations of intracellular K^+ and Na^+. During stimulation, the rise in K^+ in the synaptic space drives the Na-K exchange, and the astrocytic Na^+ decreases. Although the K^+ influx and Na^+ outflux from the Na-K pump provide competing signals for the NKCC, the Na-K pump exchanges three Na^+ ions for every two K^+ ions, so the result favors an increased NKCC influx.

At the end of the stimulus, the synaptic K^+ decreases toward baseline, so the decreased extracellular K^+ and intracellular Na^+ result in a decreased Na-K pump flux. At this time, the NKCC is required to replenish the intracellular Na^+, which means that K^+ uptake is continued via the cotransporter. At the same time, with rising intracellular K^+ and decreasing extracellular K^+, the astrocyte Kir_{AS} flux reverses, counteracting the K^+ uptake through the cotransporter. Thus, there is competition at the synaptic space between K^+ uptake by astrocyte NKCC and K^+ release by astrocyte Kir_{AS}. When the stimulus period is sufficiently long, the Na^+ has enough time to reach a low enough level that the magnitude of the NKCC flux exceeds the Kir_{AS} release, so the K^+ uptake continues beyond the point at which synaptic K^+ has reached baseline, resulting in an undershoot in extracellular synaptic K^+. The drop below baseline continues until Na^+ has risen enough for the NKCC flux to decrease, and the Kir_{AS} outflux returns the extracellular K^+ back to the baseline concentration.

Kir channel blockade

Fig. 4 shows the results when the Kir_{AS} and Kir_{AV} channels in the astrocyte are blocked. We simulate the effect of the Kir channel blocker Ba^{2+} (30) by setting the Kir currents equal to zero (see Eq. 5 and Eq. S19). The astrocyte is activated by a transient spike of K^+ in the synaptic space (Fig. 4 *c*). Under control conditions (*black curves*), the astrocyte responds with a quick rise in intracellular K^+ concentration (Fig. 4 *a*). In the presence of Ba^{2+} (*gray curves*), the astrocyte baseline K^+ is higher, and it rises more slowly to a lower peak concentration. The astrocyte membrane potential (Fig. 4 *b*) experiences a hyperpolarization in the presence of Ba^{2+} during activation and has a depolarized equilibrium value compared to the control. These results are all in good qualitative agreement with the experiments of Ballanyi et al. (30), shown here in Fig. 4, *d–f*, for comparison.

SENSITIVITY ANALYSIS

Parametric uncertainty is a major limitation of this, as well as previous (1,24,31), models. The astrocyte component alone contains 55 parameters, many of which are only crude estimates because not enough experimental data are available. To address these limitations, we perform a global parameter sensitivity analysis using the ANOVA functional decomposition and stochastic collocation (32–34), in which

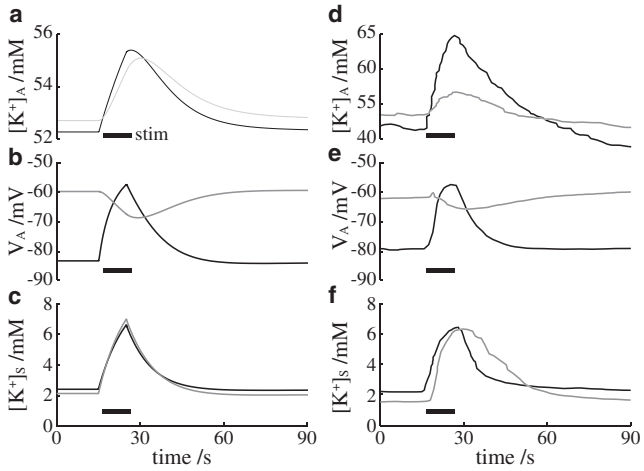

FIGURE 4 Astrocyte response to K^+ channel blocker with short stimulus spike. Black curves indicate neural-induced astrocyte stimulation under control conditions; gray curves represent astrocyte stimulation in the presence of K^+ channel blocker. (*a*) Intracellular astrocytic K^+ concentration. (*b*) Astrocyte membrane potential. (*c*) Extracellular K^+ concentration in the synaptic space. (*d–f*) Experimental results corresponding to simulation data in *a–c*, interpolated from Fig. 7 in Ballanyi et al. (30).

we vary eight key parameters simultaneously. The eight parameters were identified based on preliminary sensitivity analysis used to narrow down the 55-parameter set to the subset most critical to these experiments. Sensitivity indices are computed from the ANOVA representation in (33). The sample points are Gauss-Legendre quadrature points that come from a tensor product of the one-dimensional quadrature rule computed with the code provided in (34). In the Supporting Material, we compute the system sensitivity to all 55 parameters based on an analysis in which two parameters at a time are varied simultaneously.

The results for our 8-dimensional global sensitivity analysis are shown in Fig. 5. To understand the figure in each quadrant, consider that all eight model parameters of our subset are arranged in a large ring (to make the diagram easier to see, we have only labeled the parameters we determined to be the most sensitive). The sensitivity of a single parameter is shown as a small circle, with the diameter equal to the sensitivity of that parameter. For example, in the top left quadrant, it is shown that the potassium undershoot is most sensitive to $J_{\mathrm{NaK,max}}$ and $Rdc_{\mathrm{K^+,S}}$, the maximum pump rate of the sodium-potassium exchange and the decay rate of K^+ in the synaptic space, respectively. The fill color—white or black—of the circles indicates whether the sensitivity is constructive or destructive, respectively. In other words, when the value of $J_{\mathrm{NaK,max}}$ is increased, the undershoot is increased, whereas when $Rdc_{\mathrm{K^+,S}}$ is increased, the undershoot effect is diminished. The gray lines show the interaction of two parameters, where the thickness of the line segment is equal to the sensitivity of the interaction pair; this means that we are measuring how much the results will be changed when two parameters are changed at once. For instance, the most critical interaction pair for the undershoot is $J_{\mathrm{NaK,max}}$ and $J_{\mathrm{NKCC,max}}$, the maximum flux rate of the NKCC pump. Now that we have established how to interpret the figure, we can discuss the results in more detail.

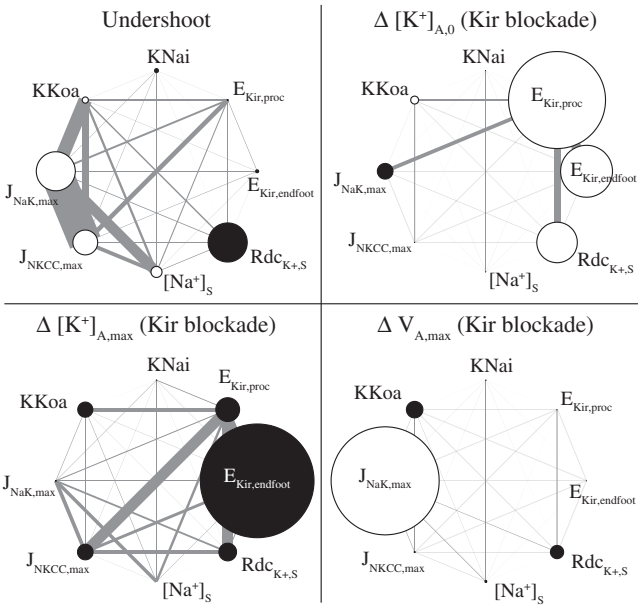

FIGURE 5 Sensitivity of K^+ undershoot and effects of the Kir blockade. Diameters of small circles indicate single-parameter sensitivity; circle color indicates whether increasing parameter magnitude will increase (*white*) or decrease (*black*) the following values: the synaptic K^+ undershoot (*top left*); the change in astrocytic K^+ after Kir blockade at baseline, $\Delta[K^+]_{A,0}$ (*upper right*), and in the active state, $\Delta[K^+]_{A,max}$ (*lower left*); the maximum astrocyte hyperpolarization, $\Delta V_{A,max}$, due to activation during Kir blockade (*lower right*). Thickness of the gray lines indicates the sensitivity of two-parameter interaction pairs.

The parameter sensitivity of the undershoot is shown in the top left quadrant of Fig. 5. We define undershoot as the amount by which the extracellular potassium in the synaptic region drops below baseline levels after a neural stimulus. The parameters $J_{\mathrm{NaK,max}}$ and $J_{\mathrm{NKCC,max}}$, the maximum flux rates of the Na-K and NKCC pumps, respectively, have the highest sensitivity (taking into account their individual sensitivity (*white circles*) and their interaction term (*thick gray rectangle*)). Both of these parameters have a positive impact on the undershoot: when either parameter is increased, the undershoot also increases. This is consistent with the hypothesis that the Na-K and NKCC pumps are responsible for the K^+ undershoot. Note also the high sensitivity of the parameter $Rdc_{\mathrm{K^+,S}}$, the decay rate of K^+ in the synaptic space. This implies that the undershoot phenomenon may be a result of factors besides the astrocyte alone, for example, changes in local synaptic activity after a period of neural activation.

In the top right quadrant, we show the sensitivity of the shift in baseline astrocyte K^+ concentration after a Kir channel blockade is applied, $\Delta[K^+]_{A,0} = [K^+]_{A,0}$ (Kir blockade) $- [K^+]_{A,0}$(control conditions). The results demonstrate that the astrocytic $\mathrm{Kir_{AS}}$ on the synapse-adjacent process is more critical in setting the baseline astrocyte K^+, whereas it is apparent in the lower left quadrant that the maximum astrocyte K^+ level depends mainly on the endfoot $\mathrm{Kir_{AV}}$.

The bottom right quadrant shows the sensitivity of the astrocyte hyperpolarization that occurs when the astrocyte is activated in the presence of a Kir blockade. Under normal conditions, the activated astrocyte would experience a depolarization due to K^+ influx through the $\mathrm{Kir_{AS}}$ channels on the synapse-adjacent processes. The only other mechanism present on the astrocyte process in this model is the Na-K exchange, which exchanges two K^+ ions into the cell for three Na^+ ions leaving the cell, an overall hyperpolarizing effect (the NKCC pump is electrically neutral, as it pumps in two positive ions, one K^+ and one Na^+, along with one Cl^{2-} ion). Thus, it is reasonable that the maximum Na-K pump flux, $J_{\mathrm{NaK,max}}$, is the most sensitive parameter for the astrocyte hyperpolarization during a Kir blockade.

DISCUSSION

Although potassium transport is accepted as a primary function of cerebral astrocytes, previous models of astrocytes

omit any description of intracellular K^+ dynamics even when electrical K^+ currents are included (1,20,24,35). Because astrocytes express Kir channels, which are sensitive to both intra- and extracellular K^+, it is necessary to model the intracellular K^+ concentration, as this affects the dynamics of the astrocyte potassium release and uptake. Notably, previous generations of this model without intracellular astrocyte potassium dynamics and Kir_{AS}/Kir_{AV} (1,24) predict a nonphysiological delay (~25 s in Farr and David (24), and 15 s in the lumped model described in the Results section) in the neurovascular response. The Kir_{AS} and Kir_{AV} included in this model accelerated the astrocytic K^+ release into the perivascular space, which helped correct the delay.

Astrocyte perivascular endfeet have been observed to express both BK channels (10,11,36) and Kir_{AV}, specifically the Kir4.1 subunit (4,7,8,37), both of which may contribute to neural-induced K^+ release into the perivascular space. Our results suggest that astrocyte endfoot Kir_{AV} may account for the initial response due to the faster activation rate of Kir_{AV} compared to BK, whereas the BK channels are responsible for sustaining the response, as their conductance is much higher than that of Kir_{AV} channels (9). According to our sensitivity analysis, the astrocyte Kir_{AS} and Kir_{AV} channels are essential to K^+ buffering (see Supporting Material).

Part of astrocyte potassium buffering is the clearance of extracellular K^+ in the synaptic region after neural activation. After extended periods of activation, the recovery to baseline K^+ is preceded by a drop below baseline levels due to extra astrocyte uptake, a phenomenon observed in vivo (5). The undershoot is most likely a result of the astrocyte K^+ uptake via NKCC and Na-K exchange, which temporarily exceeds K^+ release through Kir_{AS} (14); in fact, the undershoot is increased in Kir knockout cases (4,5). The astrocyte also has been observed to experience a hyperpolarization during the period of extracellular K^+ undershoot (38). Our results are in good agreement with these experimental findings, supporting the hypothesis that the NKCC and Na-K pumps are responsible for the undershoot, whereas the Kir_{AS} channels in the perisynaptic processes behave as a counterbalance. This is also supported by the results of our sensitivity analysis (Fig. 5, *upper left*).

It is well established that extracellular potassium affects neural health and behavior (38–41). Thus, astrocytic potassium buffering likely has both protective and functional implications in the neurovascular unit. Although astrocyte-controlled K^+ clearance from the synaptic space could be primarily a protective mechanism to prevent potassium accumulation from reaching neurotoxic levels, it is possible that astrocytes may also regulate extracellular K^+ as a means of modulating synaptic activity and overseeing neural network organization.

Rises in extracellular K^+ were observed to result in heightened neural excitability due to the increase in neural potassium ion channel reversal potential (39,42). Also observed were decreases in inhibitory GABAergic synaptic transmission in the hippocampus (41,43,44). Hippocampal CA3 neurons were found to experience a hyperpolarizing shift in the Cl^- reversal potential, resulting in greater inhibitory activity in the presence of low (below normal baseline) extracellular K^+ (41,43). Therefore, the potassium undershoot that follows long periods of synaptic activity may behave as a balancing mechanism to reduce excitability and prevent further continued activation.

Although our model was able to produce results with a good qualitative match to several different experiments, we were unable to attain a quantitative match for all of them. In particular, our model predicts a less pronounced K^+ undershoot effect than that seen in Chever et al. (5). Our sensitivity analysis offers two possible explanations: 1), because the K^+ decay rate in the synaptic space turned out to be among the most sensitive parameters to the undershoot, it is possible that other local cellular activity (e.g., changes in neural behavior) may also contribute to the undershoot; or 2) the model may be limited by the fact that it is a single compartment, meaning that any changes felt at one end of the cell will be felt immediately and entirely at the other end (see the Supporting Material). This is not physiologically likely. For instance, it is probable that electrical signals will be subject to significant loss as they propagate down the long, thin astrocyte processes. In addition to the numerous studies characterizing electrical propagation along neural dendrites, some limited data suggest that similar losses occur for electrical propagation along glial cells (45). A single-compartment model assumes that there is no loss, so a membrane depolarization that occurs at the endfoot would be grossly overestimated in terms of its effect at the end of the synapse-adjacent process. In a similar way, a multicompartment model would predict a more accurate transfer of ion concentration across the cell. In fact, recent studies have demonstrated that astrocyte intracellular ion diffusion has unique characteristics in the endfeet and processes. The same studies also revealed that isolated subcellular compartments can occur within the processes and endfeet, in which highly localized ion-concentration fluctuations occur without diffusing to or from other parts of the cell (46–48).

SUPPORTING MATERIAL

Five tables, five figures, references (49–60), model equations, and model parameters are available at http://www.biophysj.org/biophysj/supplemental/S0006-3495(13)01032-1.

The authors thank Jennifer Iddings (Georgia Regents University) and Christopher Moore (Brown University) for many helpful discussions. We also thank our anonymous referees for their constructive comments. Simulations were performed on the CCV high-performance computing cluster at Brown University.

This work was supported by the National Science Foundation Office of Cyber Infrastructure (0904288) and National Institutes of Health National Heart, Lung and Blood Institute (R01 HL089067-02).

REFERENCES

1. Witthoft, A., and G. Em Karniadakis. 2012. A bidirectional model for communication in the neurovascular unit. *J. Theor. Biol.* 311:80–93.
2. Ishii, M., A. Fujita, …, Y. Kurachi. 2003. Differential expression and distribution of Kir5.1 and Kir4.1 inwardly rectifying K^+ channels in retina. *Am. J. Physiol. Cell Physiol.* 285:C260–C267.
3. Kofuji, P., B. Biedermann, …, A. Reichenbach. 2002. Kir potassium channel subunit expression in retinal glial cells: implications for spatial potassium buffering. *Glia.* 39:292–303.
4. Neusch, C., N. Papadopoulos, …, S. Hülsmann. 2006. Lack of the Kir4.1 channel subunit abolishes K^+ buffering properties of astrocytes in the ventral respiratory group: impact on extracellular K^+ regulation. *J. Neurophysiol.* 95:1843–1852.
5. Chever, O., B. Djukic, …, F. Amzica. 2010. Implication of Kir4.1 channel in excess potassium clearance: an in vivo study on anesthetized glial-conditional Kir4.1 knock-out mice. *J. Neurosci.* 30:15769–15777.
6. Higashimori, H., and H. Sontheimer. 2007. Role of Kir4.1 channels in growth control of glia. *Glia.* 55:1668–1679.
7. Butt, A. M., and A. Kalsi. 2006. Inwardly rectifying potassium channels (Kir) in central nervous system glia: a special role for Kir4.1 in glial functions. *J. Cell. Mol. Med.* 10:33–44.
8. Higashi, K., A. Fujita, …, Y. Kurachi. 2001. An inwardly rectifying K^+ channel, Kir4.1, expressed in astrocytes surrounds synapses and blood vessels in brain. *Am. J. Physiol. Cell Physiol.* 281:C922–C931.
9. Filosa, J. A., A. D. Bonev, …, M. T. Nelson. 2006. Local potassium signaling couples neuronal activity to vasodilation in the brain. *Nat. Neurosci.* 9:1397–1403.
10. Price, D. L., J. W. Ludwig, …, M. H. Ellisman. 2002. Distribution of rSlo Ca^{2+}-activated K^+ channels in rat astrocyte perivascular endfeet. *Brain Res.* 956:183–193.
11. Girouard, H., A. D. Bonev, …, M. T. Nelson. 2010. Astrocytic endfoot Ca^{2+} and BK channels determine both arteriolar dilation and constriction. *Proc. Natl. Acad. Sci. USA.* 107:3811–3816.
12. Øyehaug, L., I. Østby, …, G. T. Einevoll. 2012. Dependence of spontaneous neuronal firing and depolarisation block on astroglial membrane transport mechanisms. *J. Comput. Neurosci.* 32:147–165.
13. Tas, P., P. Massa, …, K. Koschel. 1987. Characterization of an $Na^+/K^+/Cl^-$ co-transport in primary cultures of rat astrocytes. *Biochim. Biophys. Acta.* 903:411–416.
14. Laming, P. R. 2000. Potassium signalling in the brain: its role in behaviour. *Neurochem. Int.* 36:271–290.
15. Østby, I., L. Øyehaug, …, S. W. Omholt. 2009. Astrocytic mechanisms explaining neural-activity-induced shrinkage of extraneuronal space. *PLOS Comput. Biol.* 5:e1000272.
16. Odette, L. L., and E. A. Newman. 1988. Model of potassium dynamics in the central nervous system. *Glia.* 1:198–210.
17. Chen, K. C., and C. Nicholson. 2000. Spatial buffering of potassium ions in brain extracellular space. *Biophys. J.* 78:2776–2797.
18. Gardner-Medwin, A. R. 1983. Analysis of potassium dynamics in mammalian brain tissue. *J. Physiol.* 335:393–426.
19. Araque, A., V. Parpura, …, P. G. Haydon. 1999. Tripartite synapses: glia, the unacknowledged partner. *Trends Neurosci.* 22:208–215.
20. Postnov, D. E., R. N. Koreshkov, …, O. V. Sosnovtseva. 2009. Dynamical patterns of calcium signaling in a functional model of neuron-astrocyte networks. *J. Biol. Phys.* 35:425–445.
21. Sun, W., E. McConnell, …, M. Nedergaard. 2013. Glutamate-dependent neuroglial calcium signaling differs between young and adult brain. *Science.* 339:197–200.
22. Fernandes, J., I. M. Lorenzo, …, M. A. Valverde. 2008. IP_3 sensitizes TRPV4 channel to the mechano- and osmotransducing messenger 5′-6′-epoxyeicosatrienoic acid. *J. Cell Biol.* 181:143–155.
23. Nilius, B., H. Watanabe, and J. Vriens. 2003. The TRPV4 channel: structure-function relationship and promiscuous gating behaviour. *Pflugers Arch.* 446:298–303.
24. Farr, H., and T. David. 2011. Models of neurovascular coupling via potassium and EET signalling. *J. Theor. Biol.* 286:13–23.
25. Watanabe, H., J. Vriens, …, B. Nilius. 2003. Modulation of TRPV4 gating by intra- and extracellular Ca^{2+}. *Cell Calcium.* 33:489–495.
26. Benfenati, V., M. Amiry-Moghaddam, …, S. Ferroni. 2007. Expression and functional characterization of transient receptor potential vanilloid-related channel 4 (TRPV4) in rat cortical astrocytes. *Neuroscience.* 148:876–892.
27. Nilius, B., J. Vriens, …, T. Voets. 2004. TRPV4 calcium entry channel: a paradigm for gating diversity. *Am. J. Physiol. Cell Physiol.* 286:C195–C205.
28. Kung, C. 2005. A possible unifying principle for mechanosensation. *Nature.* 436:647–654.
29. Koenigsberger, M., R. Sauser, …, J.-J. Meister. 2006. Effects of arterial wall stress on vasomotion. *Biophys. J.* 91:1663–1674.
30. Ballanyi, K., P. Grafe, and G. ten Bruggencate. 1987. Ion activities and potassium uptake mechanisms of glial cells in guinea-pig olfactory cortex slices. *J. Physiol.* 382:159–174.
31. Bennett, M. R., L. Farnell, and W. G. Gibson. 2008. Origins of blood volume change due to glutamatergic synaptic activity at astrocytes abutting on arteriolar smooth muscle cells. *J. Theor. Biol.* 250:172–185.
32. Smolyak, S. 1963. Quadrature and interpolation formulas for tensor products of certain classes of functions. *Soviet Math. Dokl.* 4:240–243.
33. Sobol, I. M. 2001. Global sensitivity indices for nonlinear mathematical models and their Monte Carlo estimates. *Math. Comput. Simul.* 55:271–280.
34. Heiss, F., and V. Winschel. 2006. Estimation with numerical integration on sparse grids. Department of Economics Discussion paper 2006–15, University of Munich, http://econpapers.repec.org/paper/lmumuenec/916.htm.
35. Nadkarni, S., and P. Jung. 2004. Dressed neurons: modeling neural-glial interactions. *Phys. Biol.* 1:35–41.
36. Zhang, Y., and B. A. Barres. 2010. Astrocyte heterogeneity: an underappreciated topic in neurobiology. *Curr. Opin. Neurobiol.* 20:588–594.
37. Hibino, H., A. Inanobe, …, Y. Kurachi. 2010. Inwardly rectifying potassium channels: their structure, function, and physiological roles. *Physiol. Rev.* 90:291–366.
38. Walz, W. 2000. Role of astrocytes in the clearance of excess extracellular potassium. *Neurochem. Int.* 36:291–300.
39. Cressman, Jr., J. R., G. Ullah, …, E. Barreto. 2009. The influence of sodium and potassium dynamics on excitability, seizures, and the stability of persistent states: I. Single neuron dynamics. *J. Comput. Neurosci.* 26:159–170.
40. Jensen, M. S., R. Azouz, and Y. Yaari. 1994. Variant firing patterns in rat hippocampal pyramidal cells modulated by extracellular potassium. *J. Neurophysiol.* 71:831–839.
41. Thompson, S. M., and B. H. Gähwiler. 1989. Activity-dependent disinhibition. II. Effects of extracellular potassium, furosemide, and membrane potential on ECl^- in hippocampal CA3 neurons. *J. Neurophysiol.* 61:512–523.
42. Balestrino, M., P. G. Aitken, and G. G. Somjen. 1986. The effects of moderate changes of extracellular K^+ and Ca^{2+} on synaptic and neural function in the CA1 region of the hippocampal slice. *Brain Res.* 377:229–239.
43. Balena, T., B. A. Acton, …, M. A. Woodin. 2008. Extracellular potassium regulates the chloride reversal potential in cultured hippocampal neurons. *Brain Res.* 1205:12–20.
44. Jensen, M. S., E. Cherubini, and Y. Yaari. 1993. Opponent effects of potassium on GABAA-mediated postsynaptic inhibition in the rat hippocampus. *J. Neurophysiol.* 69:764–771.
45. Newman, E. A. 1987. Distribution of potassium conductance in mammalian Müller (glial) cells: a comparative study. *J. Neurosci.* 7:2423–2432.

46. Nett, W. J., S. H. Oloff, and K. D. McCarthy. 2002. Hippocampal astrocytes in situ exhibit calcium oscillations that occur independent of neuronal activity. *J. Neurophysiol.* 87:528–537.

47. Di Castro, M. A., J. Chuquet, …, A. Volterra. 2011. Local Ca^{2+} detection and modulation of synaptic release by astrocytes. *Nat. Neurosci.* 14:1276–1284.

48. Nuriya, M., and M. Yasui. 2013. Endfeet serve as diffusion-limited subcellular compartments in astrocytes. *J. Neurosci.* 33:3692–3698.

49. Hamill, O. P., and B. Martinac. 2001. Molecular basis of mechanotransduction in living cells. *Physiol. Rev.* 81:685–740.

50. Strotmann, R., G. Schultz, and T. D. Plant. 2003. Ca^{2+}-dependent potentiation of the nonselective cation channel TRPV4 is mediated by a C-terminal calmodulin binding site. *J. Biol. Chem.* 278:26541–26549.

51. Gonzalez-Fernandez, J. M., and B. Ermentrout. 1994. On the origin and dynamics of the vasomotion of small arteries. *Math. Biosci.* 119:127–167.

52. Haddock, R. E., G. D. Hirst, and C. E. Hill. 2002. Voltage independence of vasomotion in isolated irideal arterioles of the rat. *J. Physiol.* 540:219–229.

53. Hudetz, A. G., K. A. Conger, …, A. G. B. Kovach. 1987. Pressure distribution in the pial arterial system of rats based on morphometric data and mathematical models. *J. Cereb. Blood Flow Metab.* 7:342–355.

54. Cao, R. 2011. The hemo-neural hypothesis: effects of vasodilation on astrocytes in mammalian neocortex. Ph.D. thesis. Massachusetts Institute of Technology, Cambridge, MA.

55. Horiuchi, T., H. H. Dietrich, …, R. G. Dacey, Jr. 2002. Mechanism of extracellular K^{+}-induced local and conducted responses in cerebral penetrating arterioles. *Stroke.* 33:2692–2699.

56. Ngai, A. C., and H. R. Winn. 1995. Modulation of cerebral arteriolar diameter by intraluminal flow and pressure. *Circ. Res.* 77:832–840.

57. Dacey, Jr., R. G., and B. R. Duling. 1982. A study of rat intracerebral arterioles: methods, morphology, and reactivity. *Am. J. Physiol.* 243:H598–H606.

58. Parthimos, D., D. H. Edwards, and T. M. Griffith. 1999. Minimal model of arterial chaos generated by coupled intracellular and membrane Ca^{2+} oscillators. *Am. J. Physiol.* 277:H1119–H1144.

59. Taniguchi, J., S. Tsuruoka, …, M. Suzuki. 2007. TRPV4 as a flow sensor in flow-dependent K^{+} secretion from the cortical collecting duct. *Am. J. Physiol. Renal Physiol.* 292:F667–F673.

60. Metea, M. R., P. Kofuji, and E. A. Newman. 2007. Neurovascular coupling is not mediated by potassium siphoning from glial cells. *J. Neurosci.* 27:2468–2471.

Supporting Material for Potassium buffering in the neurovascular unit: Models and sensitivity analysis

Alexandra Witthoft,[†] Jessica A. Filosa,[‡] and George Em Karniadakis[*§]

[†]School of Engineering, Brown University, Providence, RI 02912
[‡]Department of Physiology, Georgia Regents University, Augusta, GA 30912
[§]Division of Applied Mathematics, Brown University, Providence, RI 02912

[*]Correspondence: Tel.: +00-1-401-8631217. E-mail: George_Karniadakis@brown.edu

S1 Detailed Model Equations

S1.1 Synaptic Space, Ω_S

When neurons are activated, they release K^+ and glutamate into the synaptic space (see Fig. 1). The governing equation for the potassium in the synaptic space is

$$\frac{\mathrm{d}[\mathrm{K}^+]_S}{\mathrm{d}t} = J_{K_s} - (J_{NaK,K} + J_{NKCC} + J_{Kir,AS})\frac{1}{VR_{sa}} - Rdc_{\mathrm{K}^+,S}([\mathrm{K}^+]_S - [\mathrm{K}^+]_{S,0}), \tag{S1}$$

where J_{K_S} is a smooth pulse approximation of potassium release from active neurons; J_{NKCC} is the astrocyte potassium uptake through the Na-K-Cl cotransport (Eq. (S7), below), $J_{NaK,K}$ is the astrocytic K^+ uptake through the Na-K pump (Eq. (S5), below), and VR_{sa} is the volume ratio of synaptic space to astrocyte intracellular space. $J_{Kir,AS} = I_{Kir,AS}/(C_{ast}\gamma)$ is the astrocytic $\mathrm{Kir_{AS}}$ flux into the perisynaptic processes (Eq. (S9), below), where C_{ast} is the astrocyte cell capacitance, and γ is a scaling factor for relating the net movement of ion fluxes to the membrane potential ([1]). $[\mathrm{K}^+]_{S,0}$ is the baseline K^+ concentration, and $Rdc_{\mathrm{K}^+,S}$ is the decay rate.

The synaptic glutamate release is assumed to be a smooth pulse, and the ratio of active to total G-protein due to mGluR binding on the astrocyte endfoot is given by

$$G^* = \frac{\rho + \delta}{K_G + \rho + \delta}, \tag{S2}$$

where $\rho = [Glu]/(K_{Glu} + [Glu])$ is the ratio of bound to unbound receptors, and δ is the ratio of the activities of bound and unbound receptors, which allows for background activity in the absence of a stimulus ([2]).

S1.2 Astrocytic Intracellular Space, Ω_{Astr}

Two astrocyte activities occur simultaneously in response to the extracellular K^+ and glutamate:

(1) The glutamate binds to receptors on the astrocyte perisynaptic process, and IP_3 production occurs inside the cell wall, causing release of intracellular Ca^{2+}, which both inhibits TRPV4 channels and triggers EET production. Both Ca^{2+} and EET activate the astrocytic BK channels, which release K^+ into the perivascular space. In addition, vessel dilation (strain, ϵ) activates the TRPV4 channels, allowing an influx of Ca^{2+} into the astrocyte.

(2) Happening concurrently, the extracellular K^+ increase leads to K^+ influx through astrocyte Na-K pump and perisynaptic $\mathrm{Kir_{AS}}$ channels, resulting in a membrane depolarization and a rise in astrocytic intracellular K^+, along with a decrease in intracellular Na^+. The NKCC influx increases with decreasing intracellular Na^+, K^+, and Cl^-; thus, the cotransport depends on the competition between K^+ influx and Na^+ outflux. This activates outward K^+ current through the perivascular endfoot $\mathrm{Kir_{AV}}$ channels, which release K^+ at the perivascular interface.

Perisynaptic processes (1)

The IP_3 production in the astrocyte is based on the model by [2] as modified by [3]:

$$\frac{\mathrm{d}[\mathrm{IP}_3]}{\mathrm{d}t} = r_h^* G^* - k_{deg}[\mathrm{IP}_3], \tag{S3}$$

where r_h^* is the IP_3 production rate, and k_{deg} is the degradation rate.

Perisynaptic processes (2)

The electrical current through the Na-K pump is carried by both Na^+ and K^+ ions, thus we treat it as the sum of these components:

$$I_{NaK} = I_{NaK,K} + I_{NaK,Na}, \tag{S4}$$

where the potassium current is carried by an influx of K^+ ions which is described by the Na-K potassium flux from [3]:

$$J_{NaK,K} = J_{NaK,max}\frac{[\mathrm{K}^+]_S}{[\mathrm{K}^+]_S + KKo_a}\frac{[\mathrm{Na}^+]^{1.5}}{[\mathrm{Na}^+]^{1.5} + KNa_i^{1.5}}, \tag{S5}$$

where $J_{NaK,max}$ is the maximum K^+ flux through the channel; the potassium concentration in the synaptic space is $[\mathrm{K}^+]_S$, and KKo_a is the threshold value for $[\mathrm{K}^+]_S$. $[\mathrm{Na}^+]$ is the intracellular sodium concentration, and KNa_i is the threshold value. VR_{sa} is the volume ratio of the astrocyte intracellular space to the synaptic space. All astrocyte

cation currents, I_{i^+}, are related to the corresponding cation concentration flux, J_{i+}, as $I_{i^+} = -J_{i^+}C_{ast}\gamma$, where C_{ast} is the astrocyte cell capacitance, and γ is a scaling factor for relating the net movement of ion fluxes to the membrane potential [1]. (For anion flux, the factor of -1 is removed). Thus, the potassium current in the astrocyte due to Na/K is $I_{NaK,K} = -J_{NaK,K}C_{ast}\gamma$. The Na-K pump exchanges 3 sodium ions for every 2 potassium ions, so the Na^+ current is

$$I_{NaK,Na} = -\frac{3}{2}I_{NaK,K}. \tag{S6}$$

The NKCC is electrically silent because its total uptake comprises two positive charges (an Na^+ and K^+ ion) for every two negative charges (two Cl^- ions): a net charge of zero. The equation for the NKCC flux is adapted from the model developed by [4]:

$$J_{NKCC} = J_{NKCC,max}\log\left[\frac{[K^+]_S}{[K^+]_A}\frac{[Na^+]_S}{[Na^+]_A}\left(\frac{[Cl^-]_S}{[Cl^-]_A}\right)^2\right], \tag{S7}$$

where the subscripts A and S indicate concentrations in the astrocyte and synaptic space, respectively, and $J_{NKCC,max}$ is the scaling factor that determines the amplitude of the pump flux. The potassium and sodium fluxes through the cotransport are $J_K = J_{NKCC}$ and $J_{Na} = J_{NKCC}$, because the cotransport mechanism carries one K^+ ion for every Na^+ ion. Because our model does not include mechanisms that interact with chloride dynamics and because the astrocytic Cl^- and Na^+ concentrations are roughly the same at baseline and active states ([4]), we add the simplification that $[Cl^-]_A = [Na^+]_A$. In addition, we also assume a constant value for the extracellular Cl^- and Na^+, $[Cl^-]_S$ and $[Na^+]_S$, respectively.

The intracellular Na^+ concentration obeys

$$\frac{\mathrm{d}[Na^+]_A}{\mathrm{d}t} = J_{NaK,Na} + J_{NKCC}, \tag{S8}$$

where $J_{NaK,Na} = -I_{NaK,Na}/(C_{ast}\gamma)$.

Astrocytes in the cortex have homomeric Kir4.1 channels and heteromeric Kir4.1/5.1 channels; both are present in the perisynaptic processes, but the endfeet express only the heteromer ([5]). Also, it is worth noting, astrocytes in thalamus and hippocampus, where there are abundant synapses, express predominantly the Kir4.1 homomer ([5]). The heteromer has a higher single channel conductance, but few data exist on the Kir channel densities along astrocyte bodies except in the retina ([6, 7]), where astrocyte function is unique and highly specialized. Therefore, we estimate the relative whole-cell Kir conductances at the endfeet and processes by adjusting for the appropriate K^+ fluxes and astrocyte membrane potential during simulation. The main difference between the Kir4.1 homomer and Kir 4.1/4.5 heteromer is the difference in their response to pH ([5]). At the moment, the model does not include a description of astrocytic pH, but when this is added at future time, it will be important to consider its nonuniform inhibitory effects on the process and endfeet Kir channels.

The current through the perisynaptic Kir_{AS} channels is

$$I_{Kir,AS} = g_{Kir,AS}(V_A - V_{Kir,AS}), \tag{S9}$$

where AS stands for the Astrocyte-Synapse interface. The channel conductance, $g_{Kir,AS}$ is calibrated to the the glial Kir4.1 data from [8]; the reversal potential, $V_{Kir,AS}$, is the Nernst potential for potassium. The conductance is defined as

$$g_{Kir,AS} = g_{Kir,S}\sqrt{[K^+]_S}, \tag{S10}$$

where $[K^+]_S$ is the potassium concentration in the synaptic space in mM, and $g_{Kir,S}$ is a proportionality constant. The reversal potential is

$$V_{Kir,AS} = E_{Kir,proc}\log\frac{[K^+]_S}{[K^+]_A}, \tag{S11}$$

where $E_{Kir,proc}$ is the Nernst constant for the astrocyte process Kir channels (about 25 mV [9]).

Astrocyte soma (1)

The astrocytic intracellular $[Ca^{2+}]$ obeys

$$\frac{\mathrm{d}[Ca^{2+}]}{\mathrm{d}t} = \beta(J_{IP_3} - J_{pump} + J_{leak}) + J_{TRP}, \tag{S12}$$

where the first three terms are Ca^{2+} fluxes from the ER into the cytosol (Eqs. (S13) – (S16) below); β is the factor describing Ca^{2+} buffering, and the Ca^{2+} influx through the TRPV4 channels is $J_{TRP} = -(1/2)I_{TRP}/(C_{ast}\gamma)$ (see Eq. (S26), below).

The calcium stores in the ER have three mechanisms for calcium transport: (1) IP_3R receptors on the ER bind to intracellular IP_3, initiating Ca^{2+} outflux from the ER, J_{IP_3} into the intracellular space; (2) a pump uptakes Ca^{2+} from the cytosol into the ER, J_{pump}, and (3) a leak flux J_{leak} from the ER into the intracellular space ([2]). The IP_3-dependent current is

$$J_{IP_3} = J_{max}\left[\left(\frac{[\mathrm{IP_3}]}{[\mathrm{IP_3}]+K_I}\right)\left(\frac{[\mathrm{Ca^{2+}}]}{[\mathrm{Ca^{2+}}]+K_{act}}\right)h\right]^3\left(1-\frac{[\mathrm{Ca^{2+}}]}{[\mathrm{Ca^{2+}}]_{ER}}\right), \tag{S13}$$

where J_{max} is the maximum rate; K_I is the dissociation constant for IP_3R binding; K_{act} is the dissociation constant for Ca^{2+} binding to an activation site on the IP_3R, and $[Ca^{2+}]_{ER}$ is the Ca^{2+} concentration in the ER. The gating variable h is governed by

$$\frac{\mathrm{d}h}{\mathrm{d}t} = k_{on}[K_{inh} - ([\mathrm{Ca^{2+}}] + K_{inh})h], \tag{S14}$$

where k_{on} and K_{inh} are the Ca^{2+} binding rate and dissociation constant, respectively, at the inhibitory site on the IP_3R. The pump flux is

$$J_{pump} = V_{max}\frac{[\mathrm{Ca^{2+}}]^2}{[\mathrm{Ca^{2+}}]^2 + K_p^2}, \tag{S15}$$

where V_{max} is the maximum pump rate, and K_p is the pump constant. The leak channel flux is

$$J_{leak} = P_L\left(1-\frac{[\mathrm{Ca^{2+}}]}{[\mathrm{Ca^{2+}}]_{ER}}\right), \tag{S16}$$

where P_L is determined by the steady-state flux balance.

The rise in intracellular Ca^{2+} in the astrocyte leads to EET production inside the cell. The EET production is governed by

$$\frac{\mathrm{d}[\mathrm{EET}]}{\mathrm{d}t} = V_{EET}([\mathrm{Ca^{2+}}] - [\mathrm{Ca^{2+}}]_{min}) - k_{EET}[\mathrm{EET}], \tag{S17}$$

where V_{EET} is the EET production rate; $[Ca^{2+}]_{min}$ is the minimum $[Ca^{2+}]$ required for EET production, and k_{EET} is the EET decay rate. Following [3], we assume that EET acts only on the astrocyte BK channels in the perivascular endfoot, rather than acting directly on the arteriole SMC as in [2].

Astrocyte soma (2)

The intracellular K^+ concentration, $[K^+]_A$, rises due to influx through Kir_{AS} and Na-K pump:

$$\frac{\mathrm{d}[\mathrm{K^+}]_A}{\mathrm{d}t} = J_{NaK,K} + J_{NKCC} + J_{Kir,AS} + J_{BK} + J_{Kir,AV} - Rdc_{\mathrm{K^+},A}([\mathrm{K^+}]_A - [\mathrm{K^+}]_{A,0}), \tag{S18}$$

where any potassium flux J is related to the corresponding electrical current I such that $J_i = -I_i/(C_{ast}\gamma)$ (for $i = [(NaK, K), (Kir, AS), BK, (Kir, AV)]$; $[K^+]_{A,0}$ is the baseline K^+ concentration, and $Rdc_{K^+,A}$ is the decay rate.

We assume in this model that the astrocyte membrane potential is uniform across the entire cell; it is likely that this is not the case, as similar membrane structures (e.g. neuronal dendritic trees) are highly lossy. However, for simplicity, we consider the astrocyte as a single electrical compartment in which the membrane potential obeys

$$\frac{\mathrm{d}V_A}{\mathrm{d}t} = \frac{1}{C_{ast}}(-I_{NaK} - I_{Kir,AS} - I_{BK} - I_{TRP} - I_{Kir,AV} - I_{leak}), \tag{S19}$$

where C_{ast} is the astrocyte cell capacitance; I_{NaK} is the Na-K pump current (Eq. (S4)), the Kir_{AS} and Kir_{AV} channel currents at the processes and endfeet are $I_{Kir,AS}$ and I_{Kir_AV} (Eqs. (S9) and (S30)) respectively; the BK current is I_{BK} (Eq. (S21), below), and the TRP current is I_{TRP} (Eq. (S26), below). The leak current, I_{leak} is

$$I_{leak} = g_{leak}(V_A - v_{leak}), \tag{S20}$$

where g_{leak} and v_{leak} are the leak conductance and reversal potential, respectively.

Perivascular endfeet (1)

Astrocytic BK channels, which occur on the perivascular endfeet, are affected by both EET and Ca^{2+}, as described by [3]:

$$I_{BK} = g_{BK} n_{BK} (V_A - v_{BK}), \tag{S21}$$

where g_{BK} is the channel conductance; v_{BK} is the reversal potential, and n_{BK} is governed by

$$\frac{\mathrm{d}n_{BK}}{\mathrm{d}t} = \phi_{BK}(n_{BK\infty} - n_{BK}), \tag{S22}$$

with

$$\phi_{BK} = \psi_{BK} \cosh\left(\frac{V_A - v_{3,BK}}{2v_{4,BK}}\right), \tag{S23}$$

$$n_{\infty,BK} = 0.5\left(1 + \tanh\left(\frac{V_A + EET_{shift}[\mathrm{EET}] - v_{3,BK}}{v_{4,BK}}\right)\right). \tag{S24}$$

Also $v_{3,BK}$ is the potential associated with 1/2 open probability, which depends on $[Ca^{2+}]$:

$$v_{3,BK} = -\frac{v_{5,BK}}{2} \tanh\left(\frac{[Ca^{2+}] - Ca_{3,BK}}{Ca_{4,BK}}\right) + v_{6,BK}, \tag{S25}$$

where $v_{4,BK}$, $v_{5,BK}$, $v_{6,BK}$, $Ca_{3,BK}$, $Ca_{4,BK}$, and ψ_{BK} are constants, and EET_{shift} determines the EET-dependent shift in the channel open probability.

In the astrocyte perivascular endfoot, the mechanosensitive TRPV4 channels allow calcium influx from extracellular space, J_{TRPV}, in response to arteriolar dilations and constrictions which stretch the enclosing endfoot membrane. These channels are also inhibited by astrocytic intracellular Ca^{2+} increases. The electrical current through the channel is

$$I_{TRP} = g_{TRP} s (V_A - v_{TRP}), \tag{S26}$$

where g_{TRP} is the maximum channel conductance; v_{TRP} is the channel reversal potential, and V_A is the membrane potential (see Eq. (S19) below). The calcium ion flux through the channel is given by $J_{TRP} = -(1/2)I_{TRP}/(C_{ast}\gamma)$. There is a factor of -1 because J_{TRP} is a flux of positive ions, whereas electrical current, I_{TRP}, always describes the motion of negative charges (an outflux of electrons being equivalent to an influx of positive ions). The factor of 1/2 is there because there are two positive charges for every one calcium ion.

The TRPV4 channel current is activated by mechanical stretches, and, after activation stops, experiences a slow decay in the absence of extracellular Ca^{2+}, and a fast decay in the presence of high extracellular Ca^{2+} ([10, 11]). Thus, we model the open probability as an ODE that decays to its variable steady state, s_∞ (Eq. (S28), below), according to

$$\frac{\mathrm{d}s}{\mathrm{d}t} = \frac{1}{\tau_{Ca}([Ca^{2+}]_P)}(s_\infty - s), \tag{S27}$$

where the Ca^{2+}-dependent time constant $\tau_{Ca}([Ca^{2+}]_P) = \tau_{TRP}/[Ca^{2+}]_P$, where $[Ca^{2+}]_P$ is the perivascular Ca^{2+} concentration (Eq. (S34), below) expressed in μM, and s_∞ is the strain- and Ca^{2+}-dependent steady-state channel open probability: We model the steady-state TRPV4 channel open probability, s_∞, by the Boltzmann equation [12, 1]:

$$s_\infty = \left(\frac{1}{1 + e^{-(\epsilon - \epsilon_{1/2})/\kappa}}\right)\left[\frac{1}{1 + H_{Ca}}\left(H_{Ca} + \tanh\left(\frac{V_A - v_{1,TRP}}{v_{2,TRP}}\right)\right)\right]. \tag{S28}$$

The first term $1/(1 + e^{-(\epsilon - \epsilon_{1/2})/\kappa})$ describes the material strain gating, adapted from [1]. The strain on the perivascular endfoot, ϵ, is taken to be the same as the local radial strain on the arteriole $\epsilon = (r - r_0)/r_0$ (see Eq. (S50), below), while $\epsilon_{1/2}$ is the strain required for half-activation. The second term describes the voltage gating and Ca^{2+} inhibitory behavior, based on the experimental results from [11] and [13]. The parameters $v_{1,TRP}$ and $v_{2,TRP}$ are the membrane potential required for half-activation and the steepness of the voltage gating curve, respectively. The inhibitory term, H_{Ca}, is

$$H_{Ca} = \left(\frac{[Ca^{2+}]}{\gamma_{Ca_i}} + \frac{[Ca^{2+}]_P}{\gamma_{Ca_e}}\right), \tag{S29}$$

where $[Ca^{2+}]$ is the astrocytic intracellular Ca^{2+} concentration (Eq. (S12)); $[Ca^{2+}]_P$ is the perivascular Ca^{2+} concentration (Eq. (S34), below), and γ_{Ca_i} and γ_{Ca_e} are constants associated with intra- and extracellular Ca^{2+}, respectively.

We point out that this TRPV4 model is a simplified description of the true TRPV4 channel, which has a highly complex and diverse range of gating properties. For instance, it has been reported that at low levels, intracellular calcium potentiates channel activity, rather than inhibiting it [14]. During a neuronal stimulus, this might affect the initial behavior of the TRPV4 channel during the brief period when the astrocyte intracellular Ca^{2+} is still low. However, both the astrocyte intracellular Ca^{2+} dynamics and the TRPV4 gating properties are not yet known with enough fine precision for a more detailed TRPV4 model to be useful. TRPV4 channels have been observed to respond to a variety of additional variables including temperature and diffusibles such as EET and IP_3 [15, 10, 13].

Thus, this model is a simplified description of TRPV4, focusing mainly on its mechanosensitive properties, as this is sufficient to capture the astrocyte response to vessel movement (refer to [16]), but additional gating properties can be added to the model in the future as more data become available.

Perivascular endfeet (2)

At the perivascular endfoot, the Kir_{AV} current is

$$I_{Kir,AV} = g_{Kir,AV}(V_A - V_{Kir,AV}), \tag{S30}$$

where AV stands for the Astrocyte-Vessel interface. The conductance and reversal potential, $g_{Kir,AV}$ and $V_{Kir,AV}$ are shown below:

$$g_{Kir,AV} = g_{Kir,V}\sqrt{[\text{K}^+]_{PV}}, \tag{S31}$$

where $[\text{K}^+]_{PV}$ is the potassium concentration in the perivascular space in mM, and $g_{Kir,V}$ is a proportionality constant. The reversal potential is again the Nernst potential, but because the channel is located at the perivascular endfoot, $V_{Kir,AV}$ depends on the perivascular K^+ concentration instead of the synaptic space concentration:

$$V_{Kir,AV} = E_{Kir,endfoot}\log\frac{[\text{K}^+]_{PV}}{[\text{K}^+]_A}. \tag{S32}$$

S1.3 Perivascular Space, Ω_P

The potassium accumulates in the perivascular space due to outflow from astrocytic BK and Kir_{AV} channels and arteriolar smooth muscle cell Kir_{SMC} channels. The equation governing perivascular K^+ is

$$\frac{\text{d}[\text{K}^+]_{PV}}{\text{d}t} = -\frac{J_{BK} + J_{Kir,AV}}{VR_{pa}} - \frac{J_{Kir,SMC}}{VR_{ps}} - R_{dc}([\text{K}^+]_{PV} - [\text{K}^+]_{P,0}), \tag{S33}$$

where VR_{pa} and VR_{ps} are the volume ratios of perivascular space to astrocyte and SMC, respectively, and $[\text{K}^+]_{P,0}$ is the resting state equilibrium K^+ concentration in the perivascular space. R_{dc} is the rate at which perivascular K^+ concentration decays to its baseline state due to a combination of mechanisms including uptake in background cellular activity and diffusion through the extracellular space. The potassium flow from the astrocyte and SMC are $J_{BK} + J_{Kir,AV}$ and $J_{Kir,SMC}$, respectively, given as $J_{BK} = -I_{BK}/(C_{ast}\gamma)$, $J_{Kir,AV} = -I_{Kir,AV}/(C_{ast}\gamma)$, and $J_{Kir,SMC} = -I_{Kir,SMC}/(C_{SMC}\gamma)$ (Eqs. (S21), (S30) and (S36), below), where C_{SMC} is the SMC capacitance.

The perivascular Ca^{2+} concentration obeys

$$\frac{\text{d}[\text{Ca}^{2+}]_P}{\text{d}t} = -J_{Ca} - J_{TRPV} - Ca_{dc}([\text{Ca}^{2+}]_P - [\text{Ca}^{2+}]_{P,0}), \tag{S34}$$

where J_{Ca} is the calcium current from the arteriole SMC (see Eq. (S47) below), and Ca_{dc} is the decay rate of perivascular Ca^{2+} concentration (similar to R_{dc}).

S1.4 Arteriole Smooth Muscle Cell Intracellular Space, Ω_{SMC}

The arteriole tone depends on the level of intracellular Ca^{2+} in the SMC (see Fig. 1) When the arteriolar Kir_{SMC} channels are activated due to perivascular K^+, the SMC membrane potential experiences a hyperpolarization, which closes Ca^{2+} channels. The decreased Ca^{2+} level in the SMC intracellular space results in a dilation, corresponding to strain, ϵ, which then activates the astrocytic TRPV4 channels.

The equations for the SMC dynamics are adopted from [17] except that the membrane potential is modified to include the Kir_{SMC} current (Eq. (S36)) following [3]:

$$\frac{\text{d}V_m}{\text{d}t} = \frac{1}{C_{SMC}}(-I_L - I_K - I_{Ca} - I_{Kir,SMC}), \tag{S35}$$

where C_{SMC} is the cell capacitance, and I_L, I_K, and I_{Ca} are the leak, K^+ channel potassium, and calcium currents, respectively (Eqs. (S42) – (S49), below).

The vascular SMC model from [17] describes vasomotion as a result of pressure-sensitive Ca^{2+} ion channel activity in the SMC (see Eqs. (S48) and (S49), below). Other models assume that vasomotion is also affected by endothelial cell activity ([1, 3]). Both the SMC and endothelial cells are likely to have a contribution to vasomotion. However, there have been observations of vasomotion in arterioles in which the endothelium was removed ([18]), indicating that the endothelium is not required for vasomotion, even if it can have an effect. Thus, for simplicity, the role of endothelial cells is not addressed here, but can be added to the model at a later time.

The potassium buildup in the perivascular space activates the arteriolar Kir_{SMC} channels according to ([3])

$$I_{Kir,SMC} = g_{Kir,SMC} k (V_m - v_{Kir,SMC}), \tag{S36}$$

where the channel conductance, $g_{Kir,SMC}$, reversal potential, $v_{Kir,SMC}$, and open probability, k, all depend on the perivascular K^+ concentration:

$$g_{Kir,SMC} = g_{Kir,0} \sqrt{[K^+]_{PV}}, \tag{S37}$$

where $[K^+]_{PV}$ is in units of mM, and $g_{Kir,0}$ is the conductance when the perivascular K^+ concentration is 1 mM;

$$v_{Kir,SMC} = v_{Kir,1} \log [K^+]_{PV} - v_{Kir,2}, \tag{S38}$$

where $[K^+]_{PV}$ is again in units of mM, and $v_{Kir,1}$ and $v_{Kir,2}$ are constants, and

$$\frac{dk}{dt} = \frac{1}{\tau_k}(k_\infty - k), \tag{S39}$$

where $\tau_k = 1/(\alpha_k + \beta_k)$, and $k_\infty = \alpha_k/(\alpha_k + \beta_k)$, in which

$$\alpha_k = \frac{\alpha_{Kir}}{1 + \exp(\frac{V_m - v_{Kir} + a_{v_1}}{a_{v_2}})} \tag{S40}$$

$$\beta_k = \beta_{Kir} \exp(b_{v_2}(V_m - v_{Kir} + b_{v_1}), \tag{S41}$$

where α_{Kir}, β_{Kir}, a_{v_1}, a_{v_2}, b_{v_1}, and b_{v_2} are constants ([3]). The SMC membrane potential is V_m (Eq. (S35)).

The leak current is simply $I_L = g_L(V_m - v_L)$, where g_L is the leak conductance, and v_L is the leak reversal potential. The K^+ channel current is

$$I_K = -g_K n (V_m - v_K), \tag{S42}$$

where g_K and v_K are the channel conductance and reversal potential, respectively. The fraction of K^+ channel open states, n is described by

$$\frac{dn}{dt} = \lambda_n (n_\infty - n), \tag{S43}$$

with

$$n_\infty = 0.5 \left(1 + \tanh \frac{V_m - v_3}{v_4}\right), \tag{S44}$$

and

$$\lambda_n = \phi_n \cosh \frac{V_m - v_3}{2 v_4}, \tag{S45}$$

where v_4 is the spread of the open state distribution with respect to voltage, and v_3 is the voltage associated with the opening of half the population, and is dependent on the Ca^{2+} concentration in the SMC:

$$v_3 = -\frac{v_5}{2} \tanh \frac{[Ca^{2+}]_{SMC} - Ca_3}{Ca_4} + v_6. \tag{S46}$$

The parameters Ca_3 and Ca_4 affect the shift and spread of the distribution, respectively, of v_3 with respect to Ca^{2+}, and v_5, v_6 are constants. The Ca^{2+} channel current is

$$I_{Ca} = g_{Ca} m_\infty (V_m - v_{Ca}), \tag{S47}$$

where g_{Ca} and v_{Ca} are the channel conductance and reversal potential, respectively. Since *fast kinetics* are assumed for the Ca^{2+} channel, the distribution of open channel states is equal to the equilibrium distribution

$$m_\infty = 0.5 \left(1 + \tanh \frac{V_m - v_1}{v_2}\right), \tag{S48}$$

with v_1 and v_2 having the same effect as Ca_3 and Ca_4 in Eq. (S46) and v_3 and v_4 in Eq. (S44). Note that in this case, v_1 is a variable that depends on the transmural pressure. We represent the relationship using this linear approximation of the data from [17]:

$$v_1 = -17.4 - 12\Delta P/200, \tag{S49}$$

where ΔP is in units of mmHg, and v_1 is in mV. For our model, we chose a value of 60 mmHg for ΔP, which we found to be consistent with experimental observations (e.g. Figure 5 in [19]) for arterioles around 50 μm in diameter, the size used in our simulations.

The SMC myogenic contractile behavior, which constricts the vessel, depends on the Ca^{2+} concentration in the SMC. The vessel circumference, x, is described by

$$\frac{\mathrm{d}x}{\mathrm{d}t} = \frac{1}{\tau}(f_{\Delta P} - f_x - f_u), \tag{S50}$$

where the radius r comes from $x = 2\pi r$; τ is the time constant, and $f_{\Delta P}$ f_x f_u are the forces due to transmural pressure, viscoelasticity of the material, and myogenic response, respectively. The myogenic force, f_u depends on the SMC Ca^{2+} concentration, which changes based on the Ca^{2+} ion channel current. These forces are discussed in detail in [17].

S2 Additional Sensitivity Analysis Results

In this section we analyze the system sensitivity to all 55 parameters using the ANOVA functional decomposition and stochastic collocation [20, 21, 22] in which two parameters at a time are varied simultaneously. (Contrast with Section 4, in which we performed a global sensitivity analysis of a subset of eight key parameters, all of which were varied simultaneously.)

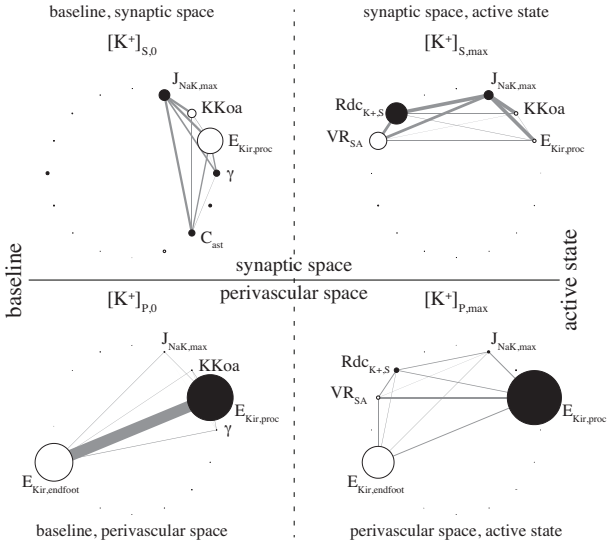

Figure S1: *Sensitivity of baseline and maximum extracellular potassium.* Small circles indicate single parameter sensitivity equal to diameter of the circle; style indicates that increased parameter magnitude will increases (*open*) or decrease (*solid*) the value of the metric: (*top left and right*) extracellular K^+ in synaptic space at baseline, $[K^+]_{S,0}$, and active state, $[K^+]_{S,max}$; (*bottom left and right*) extracellular K^+ in perivascular space at baseline, $[K^+]_{P,0}$, and active state, $[K^+]_{P,max}$, respectively. Thicknesses of grey lines indicate sensitivity of two-parameter interaction pair.

Fig. S1 shows four quadrants, each with sensitivity results for extracellular potassium concentration: The top row is the sensitivity of potassium concentration in the synaptic space, while the bottom row is the potassium concentration in the perivascular space; the left column is the baseline level, and the right column is the maximum concentration when the system is in the active state[1].

In each quadrant, consider all 55 the model parameters are arranged in a large ring, but to make the diagram easier to see, we have only labeled the parameters we have determined to be most sensitive. The data in this figure are visualized the same way as in Figure 5 from Section 4.

In the top left quadrant, the most sensitive parameters for the synaptic space baseline K^+ level are the following: $J_{NaK,max}$; $KKoa$, the threshold value of extracellular K^+ for the Na-K pump in the astrocyte process; $E_{Kir,proc}$; γ, the conversion factor relating flux of ionic concentration to electric current in the astrocyte membrane; and C_{ast}, the capacitance of the astrocytic membrane. The most sensitive parameter is $E_{Kir,proc}$, which implies that the astrocyte $\mathrm{Kir_{AS}}$ channels are the most important mechanism setting the baseline level of synaptic K^+. Likewise, in the lower left quadrant, the baseline perivascular K^+ level is most sensitive to the astrocyte endfoot $\mathrm{Kir_{AV}}$ and

[1] meaning that there is synaptic activity, which we model as a release of potassium and glutamate in the synaptic space near the synapse-adjacent astrocyte process

process Kir_{AS} channel reversal potentials ($E_{Kir,proc}$ and $E_{Kir,endfoot}$, respectively). We note that these findings are limited to an isolated astrocyte; intercellular inputs from adjacent astrocytes via gap junctions and diffusible biochemical messengers may have a profound impact impact on the results if they are included in the model.

It is worthwhile to consider baseline K^+ sensitivities (the left-hand side, top and bottom quadrants) together: note that the synaptic space and perivascular space baseline K^+ levels are both sensitive to several of the same parameters: $J_{NaK,max}$, $KKoa$, $E_{Kir,proc}$, and γ. This reveals an inherent model assumption about the connectivity of the two ends of the astrocyte, which is a possible limitation of the model. In the future, it may be necessary to upgrade the model into a multi-compartment model in which some loss exists in the propagation of ions and electric signals from one end of the cell to the other. Gap junctions between neighboring astrocytes may also need to be added to the model in the future as these would contribute to the distribution of ions throughout the glial network. The same is evident in comparing the active state K^+ in the synaptic and perivascular regions (right-hand side, top and bottom quadrants). Again, out of all 55 parameters in the model, the maximum K^+ level in the synaptic and perivascular spaces share four out of five of their top most sensitive parameters: VR_{SA}, $Rdc_{K^+,S}$, $J_{NaK,max}$, and $E_{Kir,proc}$.

S3 Simulation Parameters

Table S1: Ω_s Synaptic Space

Ω_s Synaptic Space		Description	Source
$Rdc_{\text{K}^+,S}$	0.07 s^{-1}	K^+ decay rate in synaptic space	estimation
VR_{sa}	3	volume ratio of synaptic space to astrocyte intracellular space	estimate – [3]
$[\text{Na}^+]_S$	169 mM	synaptic space Na^+ concentration	estimate – [4]

Table S2: Ω_{astr} Astrocytic Intracellular Space

Ω_{astr} Astrocytic Intracellular Space		Description	Source
astrocyte perisynaptic process			
$E_{Kir,proc}$	26.797 mV	Nernst constant for perisynaptic process Kir_{AS} channels	estimate – [9]
$g_{Kir,S}$	144 pS	proportionality constant for perisynaptic process Kir_{AS} conductance	[5]
KNa_i	1 mM	intracellular Na^+ threshold value for Na-K pump	estimation
KKo_a	16 mM		estimation
$J_{NaK_{max}}$	1.4593 mM/sec	maximum Na-K pump rate	estimation
$J_{NKCC,max}$	0.07557 mM/sec	NKCC pump rate	estimation
δ	0.001235		[3]
K_G	8.82		[3]
astrocyte soma			
r_h	4.8 μM		[3]
k_{deg}	1.25 s^{-1}		[3]
β_{cyt}	0.0244		[3]
K_{inh}	0.1 μM		[2]
k_{on}	2 $\mu\text{M}^{-1}\text{s}^{-1}$		[2]
J_{max}	2880 μMs^{-1}		[2]
K_I	0.03 μM		[2]
K_{act}	0.17 μM		[2]
V_{max}	20 μMs^{-1}		[2]
k_{pump}	0.192 μM		estimation
P_L	5.2 μMs^{-1}		[3]
$[\text{Ca}^{2+}]_{min}$	0.1 μM	minimum intracellular Ca^{2+} required for EET production	[3]
V_{EET}	72 s^{-1}		[3]
k_{EET}	7.1 s^{-1}		[3]
C_{ast}	40 pF	astrocyte membrane capacitance	[3]
g_{leak}	3.7 pS	leak channel conductance	estimation

v_{leak}	-40 mV	leak channel reversal potential	estimation
γ	834.3 mVμM^{-1}	scaling factor relating ion flux to membrane potential	[23]
$Rdc_{\mathrm{K}^+,A}$ *perivascular endfoot*	0.15 s^{-1}	astrocyte intracellular K^+ decay rate	estimation
$g_{Kir,V}$	25 pS	proportionality constant for endfoot $\mathrm{Kir_{AV}}$ conductance	[5]
$E_{Kir,endfoot}$	31.147 mV	Nernst constant for endfoot $\mathrm{Kir_{AV}}$ channels	estimate – [9]
g_{BK}	200 pS	BK channel conductance	[24]
v_{BK}	-80 mV	BK channel reversal potential	[24]
EET_{shift}	2 mVμM^{-1}		[3]
$v_{4,BK}$	14.5 mV		[3]
$v_{5,BK}$	8 mV		[3]
$v_{6,BK}$	-13 mV		[3]
ψ_n	2.664 s^{-1}		[3]
$Ca_{3,BK}$	400 nM		[3]
$Ca_{4,BK}$	150 nM		[3]
g_{TRPV}	50 pS	TRPV4 channel conductance	[25]
v_{TRPV}	6 mV	TRPV4 channel reversal potential	[26]
κ	0.1		fit to [27]
$v_{1,TRPV}$	120 mV		fit to [10, 11]
$v_{2,TRPV}$	13 mV		fit to [10, 11]
$\epsilon_{1/2}$	0.1		fit to [27]
γ_{Ca_i}	0.01 μM		fit to [11]
γ_{Ca_e}	0.2 mM		fit to [10]
τ_{TRPV}	0.9 s^{-1}		fit to [27, 11]

Table S3: Ω_P Perivascular Space

Ω_P Perivascular Space		Description	Source
$[\mathrm{Ca}^{2+}]_{P,0}$	5 μM		estimation
VR_{pa}	0.04		estimate – [3]
VR_{ps}	0.1		estimate – [3]
R_{dc}	0.2 s^{-1}	K^+ decay rate in perivascular space	estimate – [3]
$[\mathrm{K}^+]_{P,0}$	1 mM	minimum K^+ concentration in perivascular space	estimate – [3]

Table S4: Ω_{SMC} $\mathrm{Kir_{SMC}}$ Channels in Vascular Smooth Muscle Cell

Ω_{SMC} Vascular Smooth Muscle Cell Space		Description	Source
$v_{KIR,1}$	48.445 mV	factor relating $\mathrm{Kir_{SMC}}$ reversal potential to extracellular K^+	estimate – [16, 3]
$v_{KIR,2}$	116.09 mV	minimum $\mathrm{Kir_{SMC}}$ reversal potential (at low extracellular K^+)	estimate – [16, 3]
$g_{KIR,0}$	120 pS	factor relating $\mathrm{Kir_{SMC}}$ conductance to extracellular K^+	estimate – [3]
α_{KIR}	1020 sec	parameter for $\mathrm{Kir_{SMC}}$ opening rate, α_k	[3]
a_{v_1}	18 mV	parameter for $\mathrm{Kir_{SMC}}$ opening rate, α_k	[3]
a_{v_2}	6.8 mV	parameter for $\mathrm{Kir_{SMC}}$ opening rate, α_k	[3]
β_{KIR}	26.9 s	parameter for $\mathrm{Kir_{SMC}}$ closing rate, β_k	[3]
b_{v_1}	18 mV	parameter for $\mathrm{Kir_{SMC}}$ closing rate, β_k	[3]
b_{v_2}	0.06 mV	parameter for $\mathrm{Kir_{SMC}}$ closing rate, β_k	[3]

Table S5: Ω_{SMC} Vascular Smooth Muscle Cell Space

Ω_{SMC} Parameter		Source
Δ_P	60 mmHg	[28]
v_1	-23.265 mV	[17]
v_2	25 mV	[17]
v_4	14.5 mV	[17]
v_5	8 mV	[17]
v_6	-15 mV	[17]
Ca_3	400 nM	[17]
Ca_4	150 nM	[17]
ϕ_n	2.664	[17]
v_L	-70 mV	[17]
v_K	-85 mV	[17]
v_{Ca}	80 mV	[17]
C	19.635 pF	[17]
g_L	63.617 pS	[17]
g_K	314.16 pS	[17]
g_{Ca}	157 pS	[17]
K_d	1000 nM	[17]
B_T	10000 nM	[17]
α	4.3987e+15 nM C^{-1}	[17]
k_{Ca}	135.68 s^{-1}	[17]
Ca_m	170 nM	[17]
q	3	[17]
Ca_{ref}	285 nM	[17]
k_ψ	3.3	[17]
$\sigma^{\#}_{y_0}$	2.6e+06 dyne cm^{-2}	[17]
$\sigma^{\#}_0$	3e+06 dyne cm^{-2}	[17]
ψ_m	0.3	[17]

Ω_{SMC} Parameter		Source
ν_{ref}	0.24	[17]
a'	0.28125	[17]
b'	5	[17]
c'	0.03	[17]
d'	1.3	[17]
x'_1	1.2	[17]
x'_2	0.13	[17]
x'_3	2.2443	[17]
x'_4	0.71182	[17]
x'_5	0.8	[17]
x'_6	0.01	[17]
x'_7	0.32134	[17]
x'_8	0.88977	[17]
x'_9	0.0090463	[17]
u'_1	41.76	[17]
u'_2	0.047396	[17]
u'_3	0.0584	[17]
y'_0	0.928	[17]
y'_1	0.639	[17]
y'_2	0.35	[17]
y'_3	0.78847	[17]
y'_4	0.8	[17]
x_0	188.5 μm	[29]
a	753.98 μm^2	[30]
S	40000 μm^2	[30]
w_e	0.9	[17]
w_m	0.7	[17]
τ	0.2 dyne cm^{-1}	[17]

S4 Model Uncertainty

In this section, we address the uncertainty in the model by testing the effects of either omitting or modifying certain mechanisms of the model, as opposed to *parametric* uncertainty or parameter sensitivity analysis (Section S2, above, and Section 4 in the main paper).

S4.1 Astrocytic TRPV4 channels

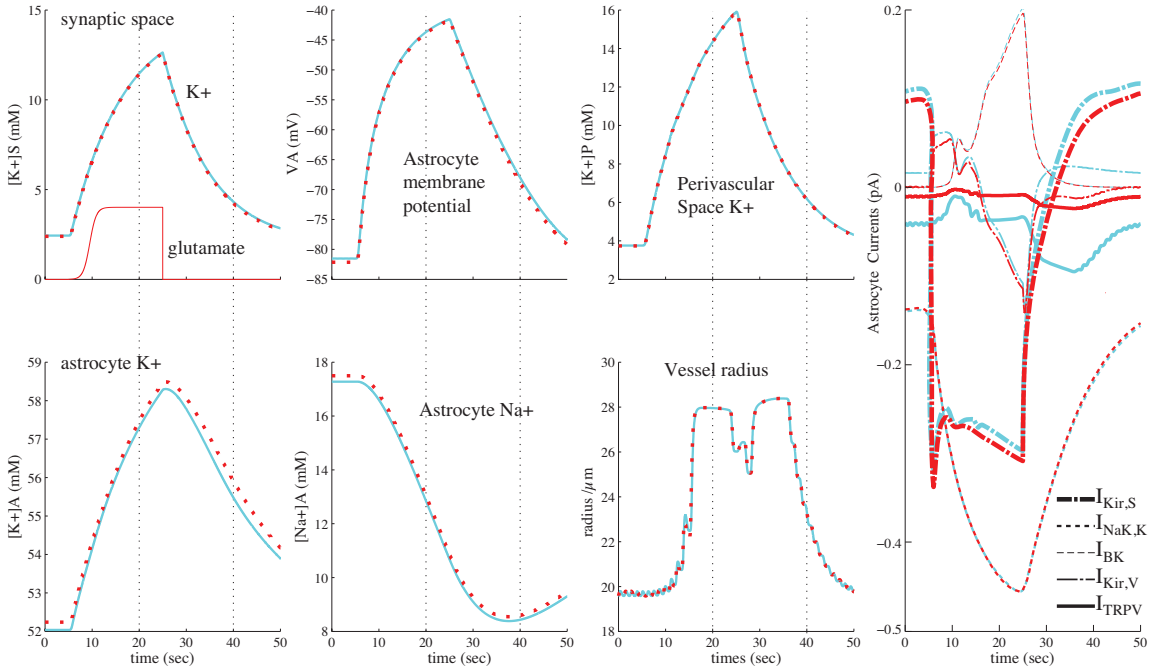

Figure S2: *Effects of TRPV4 K^+ and Na^+ effluxes.* Blue curves – original model from paper, in which TRPV4 includes only a Ca^{2+} permeability. Red curves – modified model in which TRPV4 current includes a Ca^{2+} influx as well as an outward K^+ and Na^+ component.

Because TRPV4 is a nonspecific cation channel, it is possible that it has a permeability to potassium and sodium ions [31]. In this model, we considered only the calcium component of the channel current, but we test here whether including potassium and sodium outward fluxes through astrocyte the TRPV4 channel would impact the neurovascular coupling in the simulation. Figure S2 compares the results from our model equations above (blue curves) with the results when we include K^+ and Na^+ TRPV4 currents. Because the data are limited on the specific K^+ and Na^+ permeabilities of astrocyte TRPV4, we estimate that the TRPV4 K^+ and Na^+ effluxes have equal magnitude and have a combined magnitude of 75% of the Ca^{2+} TRPV4 current. Based on our simulation results, the model is not particularly sensitive to the addition of the TRPV4 K^+ and Na^+ effluxes, as the astrocyte Kir channels, particularly at the endfoot, oppose the hyperpolarizing effects of the TRPV4 effluxes. Also, because the Kir channels are sensitive to extracellular K^+, the TRPV4 potassium efflux into the perivascular space causes a reduction in the endfoot Kir potassium release, leaving the perivascular potassium almost unchanged after adding K^+ and Na^+ effluxes to the TRPV4 model. Because of the limited data on TRPV4 K^+ and Na^+ currents and the low sensitivity of such currents in our model, we find that it is preferable to leave these out of the model, although they can be added in the future as more data are available.

S4.2 Timing of vascular response onset

In our previous paper [16], we made a correction for the time delay in the onset of vessel dilation by adjusting the Kir_{SMC} parameters. However, in this paper, we found that including astrocyte Kir channels provides a faster K^+ release mechanism from the astrocyte endfoot, thereby speeding the vessel response time by increasing perivascular potassium earlier. In Figure S3, we compare the effects of these two different "fixes."

The red curves show the results when we remove the astrocytic Kir_{AS} and Kir_{AV} from the model as in Section 3.1.1 of the main paper (see $\overline{I_{AS}}$) and we adjust the arteriole Kir_{SMC} parameters to improve the speed of the vessel response. The simulation for red curves is thus analogous to the that of our previous paper, in which the astrocyte

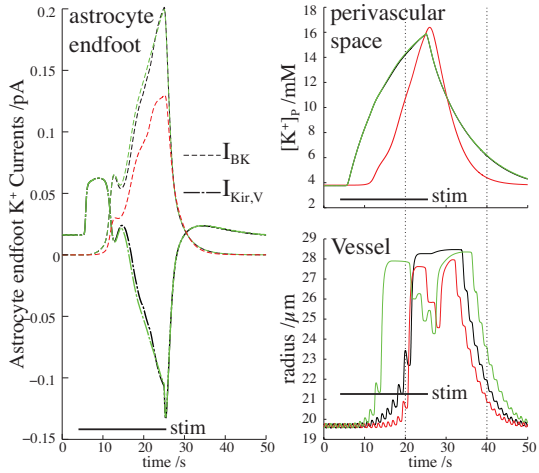

Figure S3: Left – astrocyte BK and Kir_{AV} currents. Top right – perivascular K^+. Bottom right – arteriole radius. Black bars indicate time of neural stimulus. Black curves – unadjusted Kir_{SMC} parameters; astrocyte Kir and BK currents. Red curve – adjusted Kir_{SMC} parameters, astrocyte model Kir currents excluded (see $\overline{I_{AS}}$ in Section 3.1.1 of the main paper). Green curve – inclusion of both fixes, Kir_{SMC} parameter adjustments and astrocytic Kir channels. Including both fixes does not reduce delay in the response onset, but it dramatically increases the initial speed of the dilation. The the Kir_{SMC} parameter adjustment is necessary for the vessel to constrict at >15 mM K^+, the Kir_{SMC} (green and red curves). The secondary dilation shown in these two curves occurs after the extracellular K^+ has begun its decrease, at which point, the vessel response initially favors dilation while the K^+ is still moderately high (∼8-14 mM)

model did not include Kir channels. The black curves are the results when astrocytic Kir currents are included, but there is no adjustment to the arteriole Kir_{SMC} parameters. In the plot for vessel radius vs. time (bottom right), note that although the black and red curves reach their peak values at about the same time, the black curve begins its rise several seconds earlier and initially increases at a faster rate. In addition, the red curve shows that the vessel reconstricts at a lower extracellular potassium concentration than what would be required for the black curve. The results when including both fixes are shown in the green curves: the parameters for arteriole Kir_{SMC} are the same for the green curves as for the red curves, but the astrocyte $\text{Kir}_{AS/AV}$ currents are also included. The result is that the vessel begins its dilation response at about the same time as the black curve, but at a faster rate, and it reaches its peak dilation 8-10 seconds earlier, and the vessel also reconstricts when the perivascular potassium (top right) exceeds roughly 14 mM.

The physiological rationale for including the Kir_{SMC} parameter adjustments is that they allow the vessel to respond appropriately to the level of extracellular K^+. The original parameter values used by [3] give reasonable results for higher extracellular potassium levels (10 mM and above), but they leave the vessel less sensitive to more moderate rises in extracellular potassium (4-9 mM), which is not physiologically accurate (Fig. 3 in [3] illustrates this). An overcorrection would occur if the Kir_{SMC} parameters were adjusted enough that the vessel began to respond with dilations for inappropriately low extracellular K^+.

S4.3 Role of astrocyte BK channels on neurovascular coupling

In this section we consider the effect of astrocytic endfoot BK channels on neurovascular coupling. Figure S4 shows the results from our model when the astrocyte BK channels are omitted. The top plot shows the perivascular

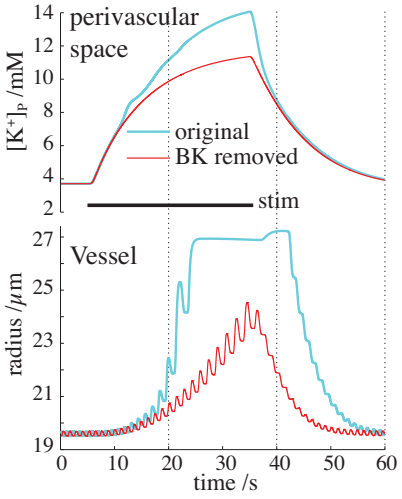

Figure S4: Astrocyte BK channel effect on neurovascular coupling. A 30 second neural stimulus occurs starting at time = 5 seconds (black horizontal bar). Blue curves – results under control conditions (with BK channels, as in main paper). Red curves – results when astrocytic BK channels are removed by setting the astrocyte Top plot – perivascular potassium concentration. Bottom plot – arteriole radius. BK conductance to 0.

potassium concentration during a 30 second neural stimulus (indicated by the black, horizontal bar), and the bottom plot shows the vessel radius. The blue curves are the results when the model is unchanged from the equations in the

main paper, and the red curves are the results when we remove the BK channels from the astrocyte model. Although the astrocyte Kir can sustain a moderate potassium efflux, without the BK channels, the perivascular potassium, and consequentially the vessel dilation, is significantly reduced according to our model.

These results seem reasonable based on the literature. A study by [32] found that the BK channel blockers paxilline and TEA inhibited astrocyte mGluR-induced outward current, which was reduced by 87.6%. Similarly, [24] found that BK channels in astrocyte endfeet produced large-conductance outward potassium currents that were activated by neural stimulation, and that blocking BK channels or ablating the gene encoding BK channels actually prevented neuronally induced vasodilation, which is believed to be caused by astrocyte release of potassium at the gliovascular space. Another study demonstrated that *rSlo* K_{Ca} (BK) channels are highly concentrated in astrocyte perivascular endfeet [33].

S4.4 Adult brain astrocyte model

Recent experimental work by [34] demonstrates a fundamental difference between astrocyte glutamate receptor expression in young and adult brains, suggesting the possibility that only astrocytes from young brains respond to synaptic glutamate release with an intracellular calcium rise. The glutamate receptor linked to IP_3 production and

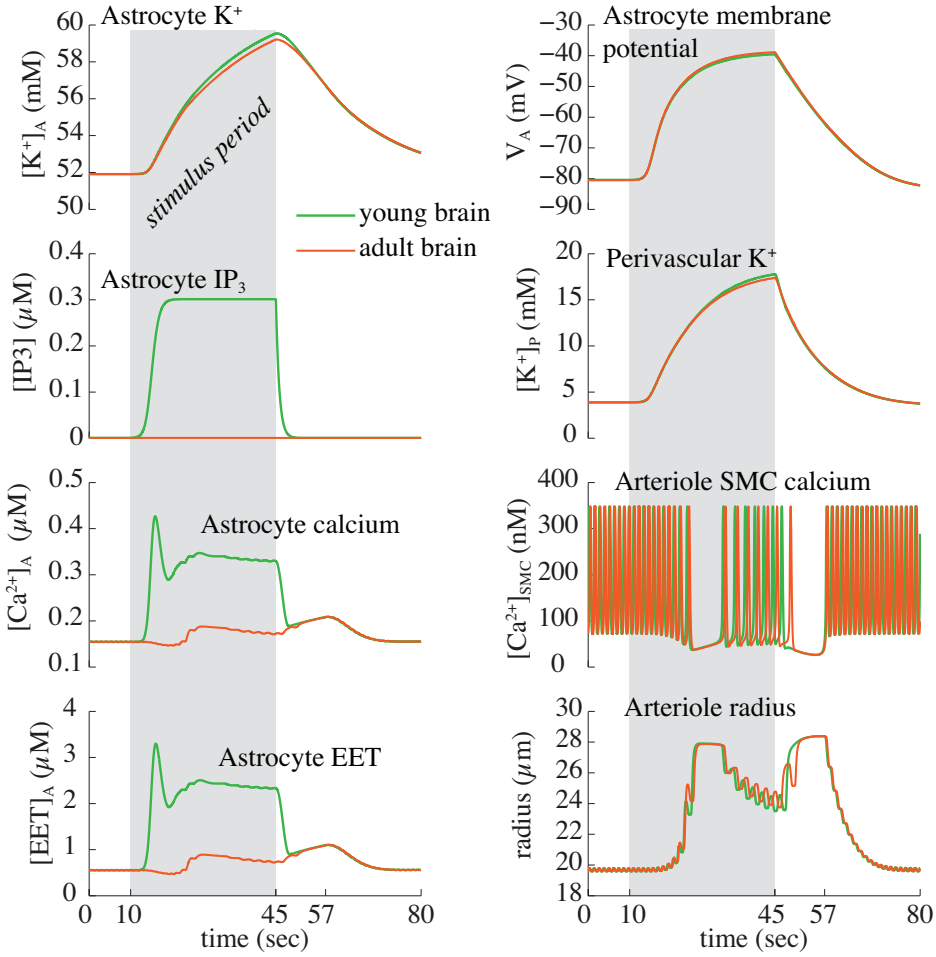

Figure S5: Comparison of young and "adult brain" astrocyte models. Green lines are the young brain model; red lines are the modified "adult" brain model. Shaded area indicates time period of neural stimulus

subsequent intracellular Ca^{2+} increase is mGluR5; the results in [34] show that cortical astrocytes from developing brains expressed mGluR5, but that both adult human and adult mouse cortical astrocytes did not. The same study found that the primary type of mGluR expressed in adult cortical astrocytes is mGluR3, which does not trigger Ca^{2+} increases.

Based on these findings we explore a possible preliminary model of an adult brain astrocyte which is a modified version of the main equations above. In the modified "adult" version of the model, we remove the glutamate triggered IP_3/Ca^{2+}/EET pathway (removing Eq. (S3) and setting $J_{IP_3} = 0$ in Eq. (S12)) that is characteristic of the mGluR5, but not mGluR3.

Results comparing the original young brain model and the modified "adult" brain model are shown in Figure S5. The green curves are from the original model, and the red curves are the results from the adult brain model. What is

interesting is that the that neural-induced vasodilation is predicted in both the young brain model and the modified "adult" model, suggesting that the astrocyte glutamate receptors may play a smaller role than expected in functional hyperemia. In fact, the modeling paper by [3] suggested that the intracellular calcium and EET rises due to astrocyte mGluR activation were necessary for vasodilation because calcium and EET both activate the BK potassium outflux at the astrocyte perivascular endfeet. They propose that astrocytic potassium "is released by endfoot BK channels due to the action of EETs on them, not due to the depolarising membrane." Upon experimenting with the equations from their paper, we found that what they propose is true for the small astrocyte depolarizations simulated in their paper. However, when we increased the amplitude of the neuronal potassium release, we found that the resulting increase in astrocyte depolarization was sufficient to activate the astrocyte BK channels even when glutamate was excluded from the simulation. Our model prediction that astrocyte-mediated neural induced vasodilation does not depend on astrocyte mGluR activity could potentially be a unifying property of astrocytes in developing and mature brains; the functional differences may have more to do with IP_3 and Ca^{2+} dependent glutamate release from astrocytes which would occur in developing brains, but not in mature brains, whose astrocytes lack mGluR5. This difference could potentially be related to what distinguishes learning in the developing and adult brains.

We also note that the above findings contradict the ideas proposed by [35]. While we recognize the importance of the work, we are cautious about dismissing astrocyte spatial potassium transfer altogether as a mechanism for neurovascular coupling. First, the experiments in [35] were performed in the retina, which is a unique and very distinctive part of the brain, and the types of astrocytes expressed in the retina are primarily fibrous, a functionally and biochemically different class from the protoplasmic astrocytes typically found in the cortex. Second, the implications of the study are slightly unclear: the authors state that astrocyte endfeet release potassium in response to depolarization. The authors also demonstrate that application of extracellular potassium near an arteriole induces a dilation. However, the paper does not focus on addressing the reason why depolarizing an astrocyte in contact with an arteriole might still fail to produce a dilation. In other words, if depolarized astrocytes release potassium from their vessel-adjacent endfeet, and if application of potassium alone dilates vessels, then why would it be that astrocyte depolarization does not dilate vessels? It seems the only possible implication is that the astrocyte does not release sufficient amounts of potassium, but the authors state in the discussion that the current injection in the experiment was large enough and localized properly on the astrocyte "ensuring that the experimentally produced depolarizations will evoke significant K^+ efflux from the endfeet." One thing that the authors do not discuss is the initial arteriole tone: if an arteriole is in or near its fully dilated state, neural stimulation or application of potassium would not cause a dilation at all (see [36]).

Supporting References

[1] Koenigsberger, M., R. Sauser, J.-L. Bény, and J.-J. Meister. 2006. Effects of arterial wall stress on vasomotion. *Biophysical Journal*. 91:1663–1674.

[2] Bennett, M. R., L. Farnell, and W. Gibson. 2008. Origins of blood volume change due to glutamatergic synaptic activity at astrocytes abutting on arteriolar smooth muscle cells. *Journal of Theoretical Biology*. 250:172–185.

[3] Farr, H., and T. David. 2011. Models of neurovascular coupling via potassium and EET signalling. *Journal of Theoretical Biology*. 286:13–23.

[4] Østby, I., L. Øyehaug, G. T. Einevoll, E. A. Nagelhus, E. Plahte, T. Zeuthen, C. M. Lloyd, O. P. Ottersen, and S. W. Omholt. 2009. Astrocytic mechanisms explaining neural-activity-induced shrinkage of extraneuronal space. *PLoS Computational Biology*. 5:e1000272.

[5] Hibino, H., A. Inanobe, K. Furutani, S. Murakami, I. Findlay, and Y. Kurachi. 2010. Inwardly rectifying potassium channels: their structure, function, and physiological roles. *Physiological Reviews*. 90:291–366.

[6] Kofuji, P., B. Biedermann, V. Siddharthan, M. Raap, I. Iandiev, I. Milenkovic, A. Thomzig, R. Veh, A. Bringmann, and A. Reichenbach. 2002. Kir potassium channel subunit expression in retinal glial cells: Implications for spatial potassium buffering. *Glia*. 39:292–303.

[7] Ishii, M., A. Fujita, K. Iwai, S. Kusaka, K. Higashi, A. Inanobe, H. Hibino, and Y. Kurachi. 2003. Differential expression and distribution of kir5. 1 and kir4. 1 inwardly rectifying k+ channels in retina. *American Journal of Physiology-Cell Physiology*. 285:C260–C267.

[8] Higashimori, H., and H. Sontheimer. 2007. Role of Kir4. 1 channels in growth control of glia. *Glia*. 55:1668–1679.

[9] Odette, L. L., and E. A. Newman. 1988. Model of potassium dynamics in the central nervous system. *Glia*. 1:198–210.

[10] Nilius, B., J. Vriens, J. Prenen, G. Droogmans, and T. Voets. 2004. TRPV4 calcium entry channel: a paradigm for gating diversity. *American Journal of Physiology Cell Physiology*. 286:C195–C205.

[11] Watanabe, H., J. Vriens, A. Janssens, R. Wondergem, G. Droogmans, and B. Nilius. 2003. Modulation of TRPV4 gating by intra- and extracellular Ca^{2+}. *Cell Calcium*. 33:489–495.

[12] Hamill, O. P., and B. Martinac. 2001. Molecular basis of mechanotransduction in living cells. *Physiological Review*. 81:685–733.

[13] Nilius, B., H. Watanabe, and J. Vriens. 2003. The TRPV4 channel: structure-function relationship and promiscuous gating behaviour. *European Journal of Physiology*. 446:298–303.

[14] Strotmann, R., G. Schultz, and T. D. Plant. 2003. Ca^{2+}-dependent potentiation of the nonselective cation channel TRPV4 is mediated by a C-terminal calmodulin binding site. *Journal of Biological Chemistry*. 278:26541–26549.

[15] Fernandes, J., I. M. Lorenzo, Y. N. Andrade, A. Garcia-Elias, S. A. Serra, J. M. Fernández-Fernández, and M. A. Valverde. 2008. IP3 sensitizes TRPV4 channel to the mechano-and osmotransducing messenger 5'-6'-epoxyeicosatrienoic acid. *Journal of Cell Biology*. 181:143–155.

[16] Witthoft, A., and G. E. Karniadakis. 2012. A bidirectional model for communication in the neurovascular unit. *Journal of Theoretical Biology*. 311:80–93.

[17] Gonzalez-Fernandez, J. M., and B. Ermentrout. 1994. On the origin and dynamics of the vasomotion of small arteries. *Mathematical Biosciences*. 119:127–167.

[18] Haddock, R., G. Hirst, and C. Hill. 2002. Voltage independence of vasomotion in isolated irideal arterioles of the rat. *The Journal of Physiology*. 540:219–229.

[19] Hudetz, A. G., K. A. Conger, J. H. Halsey, M. Pal, O. Dohan, and A. G. B. Kovach. 1987. Pressure distribution in the pial arterial system of rats based on morphometric data and mathematical models. *Journal of Cerebral Blood Flow & Metabolism*. 7:342–355.

[20] Smolyak, S. 1963. Quadrature and interpolation formulas for tensor products of certain classes of functions. *In* Dokl. Akad. Nauk SSSR, volume 4. 240–243.

[21] Sobol, I. M. 2001. Global sensitivity indices for nonlinear mathematical models and their Monte Carlo estimates. *Mathematics and Computers in Simulation*. 55:271–280.

[22] Heiss, F., and V. Winschel. 2006. Estimation with numerical integration on sparse grids. Department of Economics Discussion paper 2006-15, University of Munich, http://econpapers.repec.org/paper/lmumuenec/916.htm.

[23] Parthimos, D., D. H. Edwards, and T. M. Griffith. 1999. Minimal model of arterial chaos generated by coupled intracellular and membrane Ca^{2+} oscillators. *American Journal of Physiology-Heart and Circulatory Physiology*. 277:H1119–H1144.

[24] Filosa, J. A., A. D. Bonev, S. V. Straub, A. L. Meredith, M. K. Wilkerson, R. W. Aldrich, and M. T. Nelson. 2006. Local potassium signaling couples neuronal activity to vasodilation in the brain. *Nature Neuroscience*. 9:1397–1403.

[25] Kung, C. 2005. A possible unifying principle for mechanosensation. *Nature*. 436:647–654.

[26] Benfenati, V., M. Amiry-Moghaddam, M. Caprini, M. N. Mylonakou, C. Rapisarda, O. P. Ottersen, and S. Ferroni. 2007. Expression and functional characterization of transient receptor potential vanilloid-related channel 4 (TRPV4) in rat cortical astrocytes. *Neuroscience*. 148:876–892.

[27] Cao, R. 2011. The hemo-neural hypothesis: Effects of vasodilation on astrocytes in mammalian neocortex. Ph.D. thesis, Department of Brain & Cognitive Sciences, Massachusetts Institute of Technology, Cambridge, Massachusetts.

[28] Horiuchi, T., H. H. Dietrich, K. Hongo, and R. G. Dacey. 2002. Mechanism of extracellular K^+-induced local and conducted responses in cerebral penetrating arterioles. *Stroke*. 33:2692–2699.

[29] Ngai, A. C., and H. R. Winn. 1995. Modulation of cerebral arteriolar diameter by intraluminal flow and pressure. *Circulation Research*. 77:832–840.

[30] Dacey, R. G., Jr., and B. R. Duling. 1982. A study of rat intracerebral arterioles: methods, morphology, and reactivity. *American Journal of Physiology*. 243:H598–H606.

[31] Taniguchi, J., S. Tsuruoka, A. Mizuno, J.-i. Sato, A. Fujimura, and M. Suzuki. 2007. TRPV4 as a flow sensor in flow-dependent K^+ secretion from the cortical collecting duct. *American Journal of Physiology-Renal Physiology*. 292:F667–F673.

[32] Higashimori, H., V. Blanco, V. Tuniki, J. Falck, and J. Filosa. 2010. Role of epoxyeicosatrienoic acids as autocrine metabolites in glutamate-mediated K^+ signaling in perivascular astrocytes. *American Journal of Physiology-Cell Physiology*. 299:C1068–C1078.

[33] Price, D. L., J. W. Ludwig, H. Mi, T. L. Schwarz, and M. H. Ellisman. 2002. Distribution of rSlo Ca^{2+}-activated K^+ channels in rat astrocyte perivascular endfeet. *Brain Research*. 956:183 – 193.

[34] Sun, W., E. McConnell, J.-F. Pare, Q. Xu, M. Chen, W. Peng, D. Lovatt, X. Han, Y. Smith, and M. Nedergaard. 2013. Glutamate-dependent neuroglial calcium signaling differs between young and adult brain. *Science*. 339:197–200.

[35] Metea, M. R., P. Kofuji, and E. A. Newman. 2007. Neurovascular coupling is not mediated by potassium siphoning from glial cells. *The Journal of Neuroscience*. 27:2468–2471.

[36] Blanco, V. M., J. E. Stern, and J. A. Filosa. 2008. Tone-dependent vascular responses to astrocyte-derived signals. *American Journal of Physiology-Heart and Circulatory Physiology*. 294:H2855–H2863.